Sediment transport and beach profile evolution induced by bi-chromatic wave groups with different group periods.

José M. Alsina*
Department of Civil and Environmental Engineering
Imperial College London, SW7 2AZ London, UK. j.alsina@imperial.ac.uk

Enrique M. Padilla
Department of Civil and Environmental Engineering
Imperial College London, SW7 2AZ London, UK. e.padilla14@imperial.ac.uk

Iván Cáceres
Laboratori d'Enginyeria Marítima, Universitat Politècnica de Catalunya,
08034 Barcelona, Spain. i.caceres@upc.edu

*Corresponding author

Abstract

In this paper, large-scale experimental data are presented showing the beach profile morphological evolution induced by four different bi-chromatic wave conditions characterized by very similar energy content between them but varying the modulation period. Important differences were observed in the resultant beach profiles as a function of the wave group periods. Larger variability in the profile evolution is generally observed for larger wave group periods and, more importantly, as the wave group period increases the distance between the generated breaker bar and the shoreline increases. The measured primary wave height to depth ratio (γ) increases with the wave group period, which is consistent with the observed larger wave height at the breaking location. The primary wave

breaking location is also observed at increasing distances with respect to the initial shoreline as the wave group period increases. The variation in γ with wave group period is related to the selective energy dissipation of the higher primary frequency component (f_1) during the wave group shoaling. Broad bandwith conditions (reduced wave group period) lead to larger dissipation of wave heights at the f_1 component relative to f_2 resulting in a reduction in the wave modulation and primary wave height at the breaking location. Suspended sediment fluxes obtained from collocated velocity and sediment concentration measurements in the surf zone showed a consistently larger contribution of the mean return flow to the suspended sediment fluxes compared with the wave group and primary wave components. The distinct beach profile evolution in terms of bar location is interpreted from an increasing distance of the mean breakpoint location and the location of maximum return flow with respect to the shoreline as the wave group period increases.

Keywords: bi-chromatic wave groups, bar morphology, sediment transport, suspended sediment concentration, large scale experiments, morphodynamics.

1 - Introduction

High frequency (*hf*) wave groups and the associated low frequency (*lf*) waves are natural characteristics of random waves propagating to coastal areas. Wave grouping has important implications in coastal sediment transport and in the evolution of the coastal morphology. Measured sediment transport rates in surf zone conditions suggest a larger influence of mean components and short-scale wind and swell waves in the net cross-shore sediment transport (Ruessink et al., 1998). However, the relative importance of long waves has been showed to increase within the surf zone, as short wave dissipation occurs via wave breaking, and has

been reported to dominate the suspended sediment transport in the inner surf zone (Aagaard and Greenwood, 2008).

Moreover, beach evolution is the result of sediment transport gradients that may vary at the time-scales of long waves and wave groups. Wave groups also introduce further intermittency into the short-wave scale hydrodynamics (i.e. wave breaking, slow modulation of the water depth and wave height to water depth ratio) and the associated sediment transport pattern. Suspended sediment accumulation has been reported (O'Hara Murray et al., 2012) associated with the passage of wave groups, the so called wave pumping effect, with potential to change the short-wave and sediment suspension phase lags and the direction of the short-scale wave induced suspended sediment transport. Long waves propagate in the cross- and long-shore direction and influence processes in the 3D domain. However, in this work we will restrict our description to the cross-shore direction.

Because of the importance of *hf* wave groups and associated *lf* motions they have been extensively studied. Two mechanisms of cross-shore *lf*-motions generation from *hf* wave groups have been proposed. The first mechanism was proposed by Longuet-Higgins and Stewart (1962; 1964) and describe the generation of a water surface depression under high groups of waves in water of uniform depth by the quadratic interaction of primary waves. Longuet-Higgins and Stewart (1962) (henceforth LHS62) explain the generation of these bound waves (bound as they are forced and travel with the wave groups) in terms of the variation of the radiation stresses on the time and length scales of the short-wave groups. LHS62 solution is a steady state equilibrium solution, and in principle, is not applicable to shoaling waves. In this equilibrium situation, there should not be a net energy transfer from the primary waves to the bound wave, as there is a phase lag of 180° between the bound wave and the wave group envelope and antiphase equilibrium between the wave group forcing and the bound wave (Battjes et al., 2004).

When the *hf* wave groups propagate onto a beach, the short waves shoal and eventually break. In the shoaling process, the incoming bound long wave gains energy at the expense of the short wave energy. Usually the resulting loss of energy from the short waves is assumed to be small in comparison to the total short wave energy and is neglected. The process of bound wave growth and energy transfer from *hf* wave groups during shoaling is associated with an additional phase shift from the 180° phase lag between the wave group envelope and the bound long wave. Numerous authors have confirmed that bound long wave lags behind shoaling wave groups using field data (List, 1992), laboratory data (Battjes et al., 2004) numerical studies (van Dongeren, 1997) and analytical data (Janssen et al., 2003).

At a certain point, the short wave group will break which is linked to the second generation mechanism of *lf* motions by wave groups as explained in Symonds et al. (1982). They proposed that a time-varying breakpoint position due to incident wave groupiness radiates long waves at the group frequency both shorewards and seawards. This is because, assuming a saturated surf zone and a constant wave height to depth ratio at breaking (γ_b), higher waves in the group will break further offshore than smaller waves. The break point then acts as a wave maker generating long waves at the frequency of the break point oscillations (group frequency). If the shoreward propagating long waves reflect at the shoreline, then an interference pattern is generated and the amplitude of the final seaward propagating wave should vary according to the group frequency and surf zone width. If the phases of the reflected and breakpoint generated long waves coincide at the outer breakpoint, then constructive interference occurs and the amplitude of the total outgoing long wave is largest, leading to the maximum response (Baldock et al., 2000; henceforth B00). This occurs when the mean breakpoint location coincides approximately with a nodal point for a free standing long wave at the group frequency. In contrast, the minimum response occurs when the reflected and breakpoint generated long waves are out of phase at the outer breakpoint

location, corresponding to the mean breakpoint located close to an antinode for a free standing long wave. Laboratory results on relatively steep beaches have confirmed the "breakpoint" generation model qualitatively (Kostense, 1984) and quantitatively (Baldock and Huntley, 2002; B00) as well as numerical simulations (Madsen et al., 1997). Whereas experiments on more gentle beach slopes (Janssen et al., 2003, among others) have shown no evidence of this mechanism in forcing the long wave. Finally, van Dongeren et al. (2002) showed that the dominance of the breakpoint mechanism in forcing the long wave generation depends on the beach slope.

Although there exists an important consensus on the cross-shore *lf* motions generation and propagation, the direct influence of *lf* motions on sediment transport and beach morphology is more complicated. Many studies have linked the coastal morphology, in particular the positions and shape of bars, to the spatial scales of *lf* waves. The length scale of standing waves measured in field conditions has been shown to fit well to the cross-shore spacing of bars (Aagaard, 1990; Bauer and Greenwood, 1990; Aagaard and Greenwood, 1994; among others). This has been interpreted as a sediment particle movement from standing long wave nodes to antinodes when the dominant sediment transport mode was suspended load (Bowen, 1980; Holman and Bowen, 1982). Bauer and Greenwood (1990) and Aagaard and Greenwood (1994) have shown experimental evidence of such a mechanism. However drift velocities in the bottom boundary layer beneath standing waves are generally assumed to be small compared to *lf* and *hf* wave orbital motions and mean currents (Aagaard and Greenwood, 2008).

Moreover, because of the feedback between the morphology and the long wave hydrodynamics, it is possible that existing morphologic features (bars) force the long-wave structure rather than the other way around as proposed by Symonds and Bowen (1984). It is complicated in field conditions to establish a relationship between morphology and long-

wave pattern without comparing the same situation with and without long waves or with and without the initial forcing morphology.

Studies on the relative importance of long wave motions with respect to mean or short wave components in sediment fluxes suggest that outside the surf zone and in the outer surf zone, in general the mean and short wave components dominate the net sediment transport (Ruessink et al. 1998). However, the relative influence of *lf* motions increases in the inner surf zone as the short wave component dissipates via wave breaking. This *lf* influence has been observed in shallow waters as the wave height to water depth ratio (H/h) increases when the water depth reduces faster than the wave height and the long-wave amplitude relative to the water depth becomes important (Alsina and Caceres, 2011). An increasing *lf* influence has also been observed in the surf zone, on top of the bar crest as the mean and short wave components often cancel out (Ruessink, 1998).

The direction of the *lf* induced sediment transport seems to also show a spatial dependence. Under non-breaking conditions, numerical modeling has suggested that bound long waves tend to promote seaward sediment transport (Deigaard et al., 1999; Shi and Larsen, 1984) because of high sediment concentration induced by the largest waves within the group and the seaward bound long wave velocity due to the 180 phase lag. Local suspended sediment transport measurements in field conditions tend to support this model (Aagaard and Greenwood, 2008; Osborne and Greenwood, 1992). Inside the surf zone, no clear model exists, but long wave transport tends to be predominantly landward. Aagaard and Greenwood (2008) proposed that long waves advect sediment away from maxima in the relative incident wave height (H/h), which typically occur near the crests of longshore bars, implying a divergence of *lf* induced sediment transport at wave breakpoints (bars), which should cause destruction of the bar crest or the landward migration of the bar crest.

There are evidences of the importance of *lf* motions in beach profile morphology but there is

not yet a clear picture of the nature of this influence in terms of magnitude of sediment transport rates and direction. Coastal profile models based on a dominance of mean return flow and wave asymmetry are capable of good predictions of the cross-shore bar migration when properly calibrated while the inner surf zone morphological evolution is not as well predicted (Dubarbier et al., 2015). Similarly, recent morphodynamic models (Roelvink et al., 2009) with a description of the *lf* wave dynamics (although they also include short wave and mean return flow description) are also capable of accurately predicting the beach profile evolution.

The present paper considers this issue and investigates the influence of the wave groups and associated long waves in the beach profile evolution. Controlled large-scale experiments have been performed over the same initial beach profile configuration, and simulating different wave grouping conditions. Bichromatic waves have been generated, keeping the energy content constant but varying the wave modulation (group frequency). The mechanism behind the distinct measured profile evolution as a function of the wave group period has been analyzed. The paper is organized as follow, the description of the experimental conditions is presented in Section 2, the analysis technique and experimental results are showed in Section 3 with a discussion of the *lf* motion and wave group influence in the observed dynamic and bar migration. Finally, the main conclusions are discussed and summarized in sections 4 and 5.

2 - Experimental set up

2.1 - Wave flume and Instrumentation

The experiments were carried out in the large scale wave flume CIEM at Universitat Politecnica de Catalunya (UPC), Barcelona. This is a wave flume 100 m long, 3 m wide, and 4.5 m deep (Figure 1). The experiments were performed under the HYDRALAB-IV-

CoSSedM (Coupled High Frequency Measurement of Swash Sediment Transport and Morphodynamic) transnational access.

The working water depth was 2.5 m over the horizontal flume section but it was modified around this depth for some specific wave conditions. Two different cross-shore location reference systems are used in the present study. The first reference system is an absolute cross-shore coordinate (X_a) where the x-coordinates are referenced to an absolute fixed value, $X_a = 0$, corresponding to the lowest position of the wave paddle (this reference system is used in Figure 1). The second reference system (X) is relative to the shoreline location (x_0) at the still water level (SWL) and the initial beach profile. The relation between the reference systems is $X = X_a - x_0$. X is positive towards the emerged beach and negative towards the wave paddle.

A beach consisting of commercial well sorted sand (d_{50} = 0.25 mm, d_{10} = 0.154 mm and d_{90} = 0.372 mm) with an overall mean beach gradient of approximately 1:15 was installed. The measured sediment settling velocity is 0.034 m/s. The beach commenced 33.3 m from the wavemaker with the toe of the beach at approximately 42 m seaward of the shoreline at SWL. The range of instrumentation utilized (Figure 1) included wire wave gauges (WG) along the length of the flume, Pore Pressure Transducers (PPT) in the surf zone and Acoustic Wave Gauges (AWG) in the inner surf and swash zones. A series of Acoustic Doppler Velocimeters (ADV) and Optical Backscatter Sensors (OBS) were distributed in the surf and swash zones. The exact cross-shore location (X_a) and vertical elevation of instruments with respect to the bed level are illustrated in Table 1. Video images of selected portions of the surf and swash zones were also obtained for visual inspection. Instruments measuring water surface elevation (WG, AWG and PPT) were calibrated every 2 days by altering the water level in the flume.

The Acoustic Doppler Velocimeters (ADV), were of the type NORTEK, Vectrino, with an accuracy of ±0.5% of measured value, around ±1 mm/s. The OBS sensors were supplied by

D&A Instrument Company and the model used is the OBS 3+. OBS sensors were calibrated in-situ using sand samples from the wave flume and a recirculation tank replica of the apparatus developed by Downing and Beach (1989). The vertical elevation of the ADV and OBS instruments with respect to the bed was corrected after each test in order to keep a constant distance relative to the changing bottom.

The beach evolution along the center-line of the wave flume was measured with a mechanical wheeled bed profiler that measures both the sub-aerial and submerged beach elevation; more details can be found in Baldock et al. (2011). The vertical coordinate (z) for bed level measurements has the origin at the still-water level and is negative downward. The overall vertical profile accuracy is estimated to be of ±10 mm.

2.2 – Wave Conditions

The experimental program was divided into eight different bichromatic wave conditions. The different wave conditions were designed to have the same flux of energy and spectral energy content but different grouping period. This was done by generating bichromatic conditions with the same primary wave height of approximately H= 0.42 m and maintaining the same mean primary frequency $f_p = (f_1+f_2)/2$ = 0.27 Hz. These conditions are considered equivalent to a random wave train of peak period T_p = 3.7s and a root mean square wave height $H_{rms} = H$.

The wave conditions measured at a distance of 7.7 m from the toe of the wave paddle are illustrated in Table 2while the measured time series of water surface elevation and computed power spectrum for the different generated bichromatic conditions are shown in Figure 2. The different wave group periods are obtained by maintaining the primary mean frequency f_p constant (keeping the group velocity constant between different wave conditions) but varying f_1 and f_2. The group frequency, f_g is given by $f_g = \Delta f = f_1 - f_2$, and the group period $T_g = 1/f_g$. Broad banded groups (increasing $f_1 - f_2$ difference) lead to shorter groups (reducing T_g) where

the energy is distributed in a small number of waves. Narrow banded groups, on the other hand, lead to larger group periods and the same energy is distributed in a larger number of waves per group.

Energy peaks at the two primary harmonics f_1, f_2 and the group harmonic, f_g, are highlighted in Figure 2 with symbols. A number of sub- and super-harmonics are also visible. Super harmonics at $2f_1$ and $2f_2$ are visible corresponding to self-wave non-linear interaction during propagation (Elgar and Guza, 1985; Freilich and Guza, 1984) and also subharmonics corresponding to the triad non-linear interaction between $2f_1$ and $2f_2$ ($f = 2f_g$) and the near-resonant triads f_g and f_2 ($f = f_1 - 2f_2$).

Measured wave heights at the location close to the wave paddle showed a wave time series repeatability of around 4% on average, meaning that the targeted wave height is reproduced within 1.7cm accuracy for a 0.42 m targeted primary wave height. This accuracy is attributed mostly to small changes in the working depth due to beach porosity (the beach is reshaped and the wave flume is filled at the beginning of each wave case) since the repeatability augmented during the last tests per wave conditions (2.8%) and the standard deviation in the computed wave height reduced significantly. The working depth was constantly verified during experiments. Some discrepancies with target generation of the order of centimeters were found with larger wave period components, which means that the energy content between different wave conditions was very similar but not exactly the same with an 8% of variability. These later differences are attributed to the semi-empirical wave generation transfer function and recent variation in the wave flume bed configuration and paddle position. They promote small differences in the energy content with respect to designed. However, these small differences did not interfere with the processes being measured and the data interpretation as it will be showed. The designed wave conditions have a similar energy content to the wave conditions studied during previous experiments (Baldock et al., 2011;

Caceres and Alsina, 2016) although the initial beach slope was not the same. Dimensionless sediment fall parameter ($\Omega = H/w_sT$, where H is the primary wave height, w_s the sediment fall velocity and T the wave period) is also included in Table 2. This parameter is generally used as a descriptor of beach profile evolution and on/off-shore sediment transport dominance (Dean, 1973). Dimensionless sediment fall parameter ranged between 2.8 and 3.5. The Iribarren number is computed as $Ir = \tan\beta/\sqrt{H_0/L_0}$ where H_0 and L_0 are wave height and wave length in deep water, and illustrated in Table 2.

The generated wave components have practically the same energy content but varying group frequencies corresponding to wave group periods of 15.0 s (BE1, BE1_2), 16.7 s (BE2), 20.0 s (BE3) and 27.7 s (BE4, BE4_2). Differences in beach profile evolution and computed sediment transport will be therefore explained on the basis of changes in the wave group periods.

Every wave condition (for example BE1 case) started from the same initial beach profile, consisting on a manually-shaped 1:15 beach profile (Figure 3). For every wave condition, the same wave time series (wave realization or wave test) was repeated eight times (seven for case BE1). Each wave realization has an approximate duration of 30 min. The beach profile is measured after every wave realization. The total duration of each wave condition run is of 240 min (210 min for case BE1) with measurements of 9 profiles (8 plus the initial profile) and the measurement of hydrodynamic variables between measured beach profiles.

Some wave cases were repeated after varying the working water depth, see Table 2. Differences in the working water depth do not affect to the reference system relative to the initial SWL cross-shore coordinate (X), since differences in the working depth are already incorporated in x_0. Initial SWL positions for the different wave conditions are: x_0= 75.56 m (BE1), 75.30 m (BE1_2), 75.61 m (BE2), 75.47 m (BE3), 75.36 m (BE4) and 74.76 m (BE4_2).

2.3 - Initial beach profile

The beach profile evolution due to the wave action is a morphodynamic process with feedbacks between the beach profile changes and the hydrodynamics. Therefore, to accomplish the aim of isolating the influence of the different wave group periods in the beach profile evolution, every wave condition started from the same initial beach profile and avoided possible spurious morphodynamic effects.

The initial beach profile is formed by manually shaping the sand to obtain the initial 1/15 slope beach profile. Beach profiling is done with partly dried sand after emptying the flume. The initial profile for each wave condition is illustrated in Figure 3. Measured initial beach profiles are plotted with the vertical level starting at the still water level (SWL) and positive upwards in order to compare initial profiles at different water levels. From Figure 3, it is evident that there is only a small variability between the initial profiles for different wave conditions. The computed standard deviation between different initial profiles was always below 3 cm over the active beach profile (maximum standard deviation equal to 0.0238m) and having a minimum value of 0.01 m.

3 – Data analysis and results

3.1 – Profile evolution with different water levels under same wave condition

One of the characteristics of the present experiments is that some of the generated wave conditions were repeated after varying the water depth. Indeed, for the bichromatic test case with a grouping frequency of 0.0667 Hz (15.15 s wave group period) two working depths have been tested, d =2.53 m for BE1 and 2.48m for BE1_2, while the other bichromatic test measurements were undertaken using the same working depth of d = 2.50 m. Therefore,

before comparing the beach profile generated in different wave conditions, a comparison of the profile evolution for the two water depths under the same wave condition (BE1 and BE1_2) must be performed in order to analyze the consistency in the beach evolution.

The beach evolution and computed sediment transport at different water depths are compared using the cross-shore reference system (X) with the zero located at the SWL over the initial beach profile and the corresponding working water depth. Note that this situation, a varying water depth over a uniform beach slope, is different to a water elevation change over a natural beach with different slope configurations across the beach profile (beach-face, berm, dunes) since different beach-face configurations may vary the shoreline boundary condition (long wave reflection) having some influence in the surf-zone dynamics (Alsina et al., 2012; Brocchini and Peregrine, 1996).

Beach profiles and sediment transport rates computed for cases BE1 and BE1_2 with working depths of 2.53 and 2.48 m respectively are illustrated in Figure 4. Shoreline erosion is observed and the formation of a breaker bar. A secondary bar is also observed within the surf zone and the formation of a swash berm close to the maximum runup. The main breaker bar migrates seaward with experimentation time.

Net sediment transport rates, time-averaged per wave-test time duration, $Q(x)$, have been calculated using the sediment conservation law (Exner equation) and a known boundary condition ($Q(x)=0$) at the landward or seaward end of the profile. In the Exner equation, $Q(x)$ is given by:

$$Q(x_i) = Q(\mathrm{x}_{i-1}) - \int_{x_{i-1}}^{x_i} (1-p)\frac{\Delta z_b}{\Delta t}\,dx \qquad (1)$$

where $Q(x_i)$ is the integral volume of sediment transport (m^2/s) at position i, Δz_b is the difference in bed elevation between measurement intervals (m), Δt is the time difference between measurement intervals (s) and p is the sediment porosity, measured for the wave flume sand to be equal to 0.36. Positive $Q(x)$ values mean onshoreward sediment transport

rates, whereas negative $Q(x)$ values indicate seaward directed sediment fluxes (towards the wave paddle).

Sediment transport rates computed using Eq. (1) are corrected to obtain a zero sediment mass variation over the whole profile (sediment mass conservation), as explained in Baldock et al. (2011). The cross-shore distribution of $Q(x)$ for cases BE1 and BE1_2 is displayed in Figure 4b while the beach profile evolution is shown in Figure 4a. Small variations in the working water depth with same wave conditions (variations of 5 cm in working depth between BE1 and BE1_2) produced similar profile evolution and computed sediment transport rates. Computed differences in beach elevation between analogous profiles at the same instant of time are on average equal to 1.6 cm between profiles at BE1 and BE1_2. Differences between profiles have been computed over an active beach profile from X = -20 m to 9 m. These differences are considered low and comparable to the standard deviations obtained between the different initial profiles (equal to 1.04 cm on average). A mean BE1 profile has been obtained as the average between the measured profiles for BE1 and BE1_2 at every measuring time. This mean profile, henceforth BE1m, will be used for comparison in Section 3.2.

Differences between measured beach profiles during cases BE4 with respect to BE4_2 were of the same order of magnitude with average differences of 1.63 cm between profiles measured at a similar time instant.

3.2 – Influence of wave group period in the profile evolution

Despite the fact that the different wave conditions had similar energy content, they induced different hydrodynamic and sediment transport patterns as a result of the difference in the generated wave group periods. This, in turn, promoted different morphological evolution as illustrated in Figure 5. The final beach profiles after 7 wave realizations or 210 min of wave

action are displayed. The measured profile evolution for wave conditions BE2, BE3, BE4 is shown in Figure 5 where the working depth is 2.5 m and an average profile between BE1 and BE1_2 (see Figure 4), where the working depth is 2.48 m and 2.53 m respectively, is used. The measured final profiles show that the final bar cross-shore location is dependent on the wave group period increasing the distance with respect to the initial shoreline as the wave group period increases.

It is also noticed in Figure 5 that the wave group period has an influence on a secondary bar and in the shoreline retreat. A secondary bar is observed between the main breaker bar and the SWL (between x= -6.5 and -7.5 m) and which is equally located at an increasing distance to the SWL as the wave group period increases. The shoreline retreat is observed to reduce as the wave group period increases, although this wave group influence in the observed shoreline retreat is not as evident as in the bar location.

Other morphological differences of the final beach profiles induced by the different bichromatic wave groups are shown within the swash area where the berm location tends to appear further seaward as the wave group period increases, although cases BE2 and BE3 did not display a very significant berm. In general, larger shoreline erosion was measured under the smaller group periods.

Net sediment transport rates computed using the Exner equation, Eq. (1), after the final experimentation time is displayed in Figure 6 and further illustrates the distinct morphological features with a varying wave group period.

The breaker bar crest location has been computed as the cross-shore location where a local maximum in the measured bed elevation exists, i.e. the beach profile inflection point at the surf zone. The time evolution of the bar crest location with respect to the initial SWL location for the different bichromatic wave conditions is illustrated in Figure 7. There are differences in bar crest locations, increasing in distance relative to the initial shoreline as the grouping

period increases. Moreover, a larger variability in the bar migration is evident, with larger bar location changes in time, as the wave group period increases (i.e. the bar for BE4 case migrates 2 m in 210 min, starting from a crest located at X~10.45 m to X~12.5 m while the bar for case BE1 migrates only 0.5 m during that period of time).

It is also interesting that the bar crest migration tends to a relatively stable situation with small variations in bar x-location after a certain period of time. This "relatively" stable situation is reached after approximately 2 h of experimentation time for BE1 case, 2.5 h for BE3 case and 3.5 h for BE4 case. The wave group period then has an influence on the beach profile evolution, reflected in the beach profile changes in time (breaker bar location) and in the time that the beach profiles evolution need to reach to a *quasi-equilibrium* situation.

This suggests a larger variability in the profile evolution for narrow bandwidth bichromatic conditions (larger modulation and wave group periods) while broad band conditions (smaller wave group periods) seem to reach a *quasi-equilibrium* condition faster. A further example of such an increasing variability will be illustrated in Figures 10c and 11c in which the bed level change during 210 mins of experimentation time is displayed for cases BE1m (Figure 10c) and BE4 (Figure 11c). Clearly the narrow bandwidth case (BE4) shows a larger variability in the overall bed evolution.

3.3 – High frequency wave breaking

Wave heights are obtained directly from spectral analysis. Therefore, H_1, H_2 and H_g are obtained as the wave height associated with frequency components 1, 2 and the group frequency. The primary wave height, H is also defined associated with the incident high frequency components 1 and 2.

The spectrum density of the water surface elevation is computed using the fast Fourier transform function without windowing or averaging. Wave height to water depth ratios have been computed from the measured incident primary wave components, $\gamma = H/h$ where h is

the total water depth, $h = d + \bar{\eta}$ including the measured mean water surface elevation, $\bar{\eta}$ (set-down and set-up), with d the water depth to the still water level. Wave height to water depth ratios, γ, have been traditionally used as a parameter to evaluate wave evolution and energy saturation in the surf zone, and as a breaker criterion, γ_b, is important in many wave transformation models (Alsina and Baldock, 2007; Battjes and Janssen, 1978).

Figure 8 displays the γ-distribution versus water depth, h, non-dimensionalised by H_0 (where H_0 is the wave height measured at generation) up to the primary wave height breaking location (Figure 8b), within the inner surf zone (Figure 8a) and the γ-distribution versus cross-shore location (Figure 8c). Note that the x-axis in Figure 8c is decreasing and the shoreline is on the left. The γ-distribution in the cross-shore profile showed a double-peak distribution for every wave condition with a maximum at the primary breaking location and another maximum in the inner surf zone associated with a secondary wave breaking due to the smaller waves within the group breaking closer to the shoreline (inner breaking). The primary wave breaking location is interpreted as the location where all waves within the wave group larger than the primary wave height (H) are already breaking. The primary and inner wave breaking locations are precisely obtained as the locations, within the surf zone, where γ achieves a maximum value. The primary and inner breaking locations for each wave condition are indicated in Figure 8c with vertical arrows. After the initial wave breaking, γ-values decay and, within the inner surf zone, γ peaks again at the inner breaking location as illustrated in Figures 8a and 8c. The scatter in Figure 8a is due to the bar and through presence. After initial wave breaking and γ-values decay, γ is often still relatively high at the landward side of the bar due to small water depths despite of the wave height decay. The through presence after the bar is responsible of small γ-values at small h/H_0 values. The mean wave breaking location $\bar{X}_b$ is defined as the mean between the primary and inner wave

breaking location.

From the measured data, a trend of larger γ values at the primary wave height breaking location as the wave group period increases is observed. This is confirmed by a second order polynomial fit-to-data (also illustrated in Figure 8b) that shows such tendency with a γ variability from 0.95 for BE1 cases to 1.2 for BE4 cases. This translates to an increase in the wave breaking height as the wave group period increases but also, the primary breaking cross-shore location is observed at increasing distances relative to the initial SWL position (see Figure 8c).

3.4 – Ingoing-outgoing long wave separation

The wave motion at the primary waves and wave group frequencies has been studied to highlight the wave group influence on the observed profile morphological evolution and to analyze the influence of wave generation (lack of active absorption of low frequency motions). The long wave (wave group period) motion consists of a bound wave, which travels with the wave groups, an ingoing free wave (generated or reflected at the wave paddle) and an outgoing free long wave (radiated or reflected at the surf zone or shoreline). In the constant depth section of the wave flume (X_a < 34 m), the amplitudes of the bound long wave, free incident long wave and free outgoing long wave at the wave group frequency (f_g) have been separated using the methodology proposed by Kostense (1984) and three sensors located at X_a = 7.72 m, 28.48 m and 30.55m. Kostense's methodology is especially suitable for bichromatic wave conditions on a plane bed (close to the wave paddle) and is preferred versus other methodologies (Battjes et al., 2004) because of the spatial resolution between wave gauges in the present tests, Battjes et al. (2004) requires a higher spatial resolution than used here, or the lack of enough velocity measurements to use the methodology proposed by Sheremet et al. (2002).

Measured incident bound wave separated with Kostense (1984) methodology is compared

with the theoretical incident bound wave computed using the LHS62 formulation. Figure 9a displays the measured and computed theoretical bound wave using LHS62 where a good overall agreement is observed between the measured and theoretical bound wave.

The measured outgoing long wave as a function of χ parameter (Symonds et al., 1982), is displayed in Figure 9b, the χ parameter is computed as $\chi = \omega^2 \bar{X}_b / g\beta$ where ω is the angular group frequency, β is the beach slope, g is gravity and $\bar{X}_b$ is the mean wave breaking location, computed from analysis of measured wave height and water depth as explained in section 3.3. The amplitude of the outgoing free long wave at the group frequency shows an overall increase as χ grows up to a χ value ≈ 1.6 where the outgoing amplitude seems to decrease, although the data scatter is high. A similar trend is shown in Madsen et al. (1997) using numerical modeling and B00 from experimental data with a maximum outgoing amplitude at χ = 1.2. The discrepancy on the χ value may be due to the methodology to obtain the wave breaking location (a mean breaking location from visual observations in B00, versus a mean observed wave height to water depth ratio in this analysis).

The influence of *lf* motions re-reflected (or *seiching*) at the wave paddle has also been analyzed. *Seiching* has been observed in this wave flume with similar initial beach profile configuration but random energetic conditions occurring with a typical frequency of 0.022 Hz (Alsina and Cáceres, 2011). Analyzing the measured water surface signal when the wave paddle stopped generation showed some energy at this frequency, however it is negligible compared to the incident energy at any other frequency.

Re-reflection of *lf* energy at the wave group frequency at the wave paddle is also expected. The Kostense (1984) method of separation allows the separation of any free incident wave at the group frequency for bichromatic conditions. Any long wave, at the group frequency, reflected at the wave paddle propagates as a free incident wave and is theoretically separated using Kostense's method. The incident free long wave amplitude was shown to be of the

same order as the outgoing free long wave indicating that seiching was indeed present. However existing seiching was found to be small relative to the total low frequency energy within the surf zone as will be explained in the next section and in the discussion.

3.5 – Cross-shore distribution of wave height at different frequencies

In this section, the wave heights at different frequencies and its cross-shore distribution will be presented. The cross-shore distribution of the wave height at the short wave components f_1 and f_2 are showed in Figure 10a for cases BE1 and BE1_2 and in Figure 11a for case BE4. Wave heights are averaged using the first 7 measured hydrodynamics runs. The wave height variability between hydrodynamic runs is illustrated with a shaded plot and the mean value is indicated with a solid line. Larger variability between hydrodynamic runs is showed for the narrow banded condition (BE4) due to the larger variability in the morphological evolution. Cases BE1 and BE1_2 are plotted together relative to their respective initial shoreline location (x_0) showing very good agreement. The wave breaking region delimited by the primary and inner breaking locations computed as the maximum γ-values within the surf zone is displayed in the background as a shaded area and vertical dashed lines.

The wave height associated with the group frequency (f_g) is also displayed in Figures 10b and 11b. The last cross-shore point in the wave height at f_g is computed from the power spectrum of the computed shoreline vertical oscillation and plotted at the mean shoreline location. The shoreline vertical elevation is obtained using the acoustic sensors (AWG) located in the swash zone interpolating the water surface elevation measured at different locations over the measured beach profile. This is possible thanks to the good spatial resolution in acoustic sensors in the swash area (8 AWG with a separation of 0.9 m on average, the accuracy is then of ±0.45m in the cross-shore location, ±0.03 m in the vertical elevation). An analytical solution for a standing wave is also shown in Figures 10b and 11b. The standing wave

solution is given by a zeroth order Bessel function (J_0) with a shoreline amplitude equal to that measured, and with origin at the mean cross-shore run-up position.

Finally, the bed level changes, obtained as $\Delta z = z_i - z_0$ (where z_i is the bed elevation measured at each instant of time and z_0 is the initial bed level), are also showed in Figures 10c and 11c for cases BE1 and BE4 respectively. The bar crest locations computed as the profile inflection points are indicated in figures with "○" symbols.

The *hf* wave height cross-shore distribution (Figures 10a and 11a) shows a dissipation of f_1 and f_2 components during shoaling with larger dissipation comparatively for the shorter (in period) primary component, f_1. The f_1 component decay is also associated with an increase in energy at group frequency (f_g) and $2f_g$ component (heights at $2f_g$ not shown for clarity). More importantly, this energy decay is more pronounced in the BE1 case (Figure 10a) where the frequency difference between components is larger (broader bichromatic condition) than BE4 (see Figure 11a). This pattern of energy transfer from high frequency components to subharmonics has been previously reported in other bichromatic conditions (B00; Baldock, 2012) with larger energy transfer occurring for the higher short wave frequency component and a significant reduction of the short wave amplitude during shoaling. Similarly, related to the selective energy dissipation of f_1 in case BE1, it is observed a primary wave height decay during shoaling (Figure 10a), before wave breaking, which is not detected in case BE4 where the primary wave height during shoaling are almost constant up to wave breaking (Figure 11a). This would support observations of earlier wave breaking and larger primary wave heights observed for narrow banded cases (BE3 and BE4).

This is further illustrated in Figure 12 where ensemble averaged time distribution of water surface elevations for cases BE1 and BE4 are illustrated for different cross-shore locations. Ensemble averaging has been performed at the repetition period (T_R). The repetition period is the time at which the phase of an individual wave within the group repeat exactly (B00). For

most of the cases (BE2, BE3 and BE4), the bichromatic conditions were designed in a manner that the repetition period was coincident with the group period, i.e. every wave group repeated exactly in time. However, this was not possible for the conditions of case BE1 (a wave group period of around 15 s with a similar energy content than the rest of the cases). For this case, the repetition period is around 198 s.

Figure 12 shows water surface elevation (ensemble averaged) time series over a time span of 50 s (i.e. two wave group periods for BE4 condition and approximately 3 wave groups for BE1 case). Wave condition BE1 is displayed in Figures 12 a), b) and c) at cross-shore locations, X = -67.85 m, -9.96 m and -7.83 m respectively while wave condition BE4 is displayed in Figures 12 d), e) and f) at cross-shore locations X = -67.64 m, -9.75 m and -7.62 m respectively. Wave breaking is occurring at around X = -12.73 m (BE4) and X = -9.96 m (BE1). This is evident comparing Figures 12b) and 12e) where largest waves within the group in case BE4 (Figure 12e) are already breaking. However for case BE1 (Figure 12b) the largest waves keep the wave height and only changes in the wave asymmetry and shape are observed. Moreover, wave condition BE4 seems to keep the wave group modulation at the different cross-shore locations (see Figure 12f compared to 12d) while wave condition BE1 is losing modulation (see Figure 12c compared to 12a) consistent with a faster reduction in H_1 relative to H_2.

The long wave cross-shore pattern at the group frequency, illustrated in Figures 10b and 11b, is characteristic of incident and outgoing long waves where the outgoing long wave is originated at the surf zone (and radiated seaward) and/or onshoreward (reflection). A standing pattern is evident at the shoaling region for the case BE1 resultant of the ingoing and outgoing wave heights. For the BE4 case this pattern is not evident denoting a progressive long-wave structure dominated by the ingoing bound long wave. This is consistent with smaller outgoing amplitudes measured for case BE4 than for BE1 (Figure 8b). The mean

breakpoint position for case BE1 corresponds approximately to a nodal point for a free standing long wave at the group frequency displayed by the Bessel function in Figure 10b, constructive interference between radiated and reflected low frequency motions occurs and the total breakpoint forced free long wave attains maximum amplitude as observed in the present experiments. This situation is denoted as *maximum response* in B00 and occurs for χ values close to 1.2. The mean breakpoint location for case BE4 corresponds approximately to an antinode location and the reflected long wave is out of phase with any possible long wave radiated at the breakpoint location. The total outgoing amplitude is reduced and the long wave cross-shore structure is dominated by the incident bound wave. This situation is denoted as minimum response in B00.

Figure 13 shows the phase lag ψ of the low frequency surface elevation with the high frequency groups envelope (Figure 13a for case BE1 and Figure 13b for case BE4) and the phase lag of the low frequency surface elevation at consecutive cross-shore locations (Figure 13c for case BE1 and Figure 13d for case BE4). Two nodal locations are observed for case BE1 at X ≈ -20 m and X ≈ -3 m and an antinode at X ≈ -10 m. The mean breaking location is then located between an antinode (seaward of the breakpoint location) and a nodal location (onshoreward of the breakpoint). In contrast, wave condition BE4 shows virtually no cross-shore nodal structure at the group frequency. This is because the outgoing long wave amplitude is relatively small as discussed and the total wave amplitude at f_g is dominated by the incident bound long wave. The *lf* wave is out of phase with the wave group envelope in the shoaling region (Figure 13b) up to the breaking point. From this location to the shoreline the phase lag reduces progressively consistent with an inversion of the groupiness after wave breaking as, on average, the highest wave before breaking is the lowest after breaking (Svendsen and Veeramony, 2001).

The bar generation and migration illustrated in Figures 10c and 11c shows a larger variability

in the bed evolution for the narrow band condition (BE4) in comparison with the bed evolution measured for the broad band condition (BE1). For the BE1 case, the breaker bar tends to be located close to an antinode location of the long-wave standing pattern while the secondary bar is located close to a nodal location. The former has been previously reported by Bauer and Greenwood (1990) and Aagaard and Greenwood (1994). However, the bar and the anti-node location for case BE1 is also coincident with the primary wave height breaking location in the present experiments. On the contrary, for case BE4 (Figure 11c), the bar also generates without the presence of any nodal location.

3.6 – Sediment suspension at the wave group time scale

Within the surf zone, collocated measurements of water surface elevation, flow velocity and suspended sediment concentration were available.

Figure 14 shows the ensemble average of water surface elevation, horizontal flow velocity and suspended sediment concentration (SSC) at the location X =-4.13 m within the surf zone for the BE1 case. Ensemble averaging has been done using the last 6 measured hydrodynamic runs for each wave conditions. This location is eroding as illustrated in Figure 4a. Most of the waves arrive as broken waves to this location. The wave group modulation is not as evident in the water surface elevation signal as in the generation area (Figure 2a). This is attributed to the larger reduction in f_1 relative to f_2 for case BE1 before breaking (Figure 10a) and thus reducing wave modulation, the wave heights become more uniform as the energy of one of the primary components reduces. The energy at the group frequency is important in this location relative to the incident primary components. Low-pass filtered water surface elevation and velocity are illustrated in Figure 14 with a dash-dotted line. It is observed that the highest waves within the *hf* wave groups are in phase with the *lf* water surface oscillation. The reason behind this is attributed to the inversion in the wave modulation after breaking

(Svendsen and Veeramony, 2001; Janssen et al., 2013) but also to the standing long wave pattern within the surf zone and the outgoing influence in the filtered signal (see Figure 13a).

A strong modulation of the flow velocity at the group frequency is also observed. There is a slight phase lag between the *lf* induced water surface elevations and velocity, this phase lag is more noticeable at other locations closer to the shoreline due to the ingoing-outgoing influence in the *lf* induced velocity (Elgar and Guza, 1985) and the standing pattern discussed in the previous section.

The suspended sediment concentration is partly controlled by the group frequency modulation. High waves within the group tend to be coincident with high sediment suspension events, however the highest wave does not always promote the largest suspension event and not all the wave groups promote the same sediment suspension pattern. This suggests inertial effects and time history influences on the sediment suspension response to hydrodynamics. The resultant suspended sediment flux is predominantly negative (seaward directed) with a time averaged sediment flux $\langle uc \rangle$=-4.257×10^{-4} m/s due to the negative predominant velocities at the measuring location (mean return flow). The standard deviation resultant from the ensemble averaging is relatively low for the water surface elevations and velocities but larger for the ensemble averaged suspended sediment concentration as it is expected due to the "apparently random" sediment suspension nature. Different locations within the inner surf zone, in cases BE1 and BE1_2, show a similar picture to Figure 14.

A similar plot for the BE4 case (same cross-shore location) is illustrated in Figure 15 where two wave group periods are shown for clarity. The location is also within the inner surf zone at X = -3.51 m. Case BE4 shows a larger modulation in the water surface elevation in comparison with case BE1. Wave groups are similarly in phase with the *lf* water surface elevation. In this case, the long wave water surface oscillation is not in phase with the lf-induced velocities due to the larger influence of ingoing long wave. The influence of

individual waves in the flow velocity pattern is more noticeable than in case BE1.

Sediment suspension events appear related to individual waves forming the wave groups. However, the magnitude of the single suspended sediment events is controlled by the modulation of the water surface elevation showing higher peaks close to the crest of the *lf* signal and a modulation of the base SSC signal correlated with the *lf* water surface. Similar to condition BE1, the overall suspended sediment flux is negative with a time averaged sediment flux $\langle uc \rangle$=-4.479×10^{-4} m/s due to the mean negative velocity. This location is also eroding as illustrated in Figure 5a. Interestingly the time-dependent sediment transport rate for both cases, BE1 and BE4, shows an important low frequency modulation but the positive and negative long wave sediment transport rates are of similar magnitude but with opposing direction and tend to balance each other. Thus, the mean sediment transport rate dominates.

3.7 - Relative contribution of short wave, long wave and mean component to the suspended sediment fluxes

In the previous subsection the hydrodynamic forcing and sediment suspension events have been shown at the temporal scale. The relative contribution of the different components to the total sediment fluxes will be analyzed in this subsection.

Using the collocated measured time series of velocity and suspended sediment concentration at three different locations within the inner surf zone (see Figure 1 for details on instrument locations), sediment fluxes induced at different time scales of motion have been studied. ADV and OBS sensors are located at the same vertical elevation with respect to the bed level at the beginning of each hydrodynamic run. Bed level variations within each hydrodynamic run are of the order of centimeters in these locations reducing as the beach profile tends to equilibrium. Therefore, only the last 6 hydrodynamics runs, where the bed level changes are

smaller, are used to compute sediment fluxes.

Time series of horizontal velocity and sediment concentration can be decomposed into a mean and an oscillatory component. The net time averaged sediment flux (q_{net}) can be expressed as:

$$q_{net} = \langle uc \rangle = \bar{u}\,\bar{c} + \langle \tilde{u}\tilde{c} \rangle \tag{2}$$

where the brackets indicate time averaging over the measuring time, the – overbar denotes mean component and the ~overbar indicates oscillatory components. The oscillatory component can be also divided into high and low frequency components denoted with *hf* and *lf* sub-index respectively. Then the total net transport is expressed as:

$$q_{net} = q_m + q_{hf} + q_{lf} = \bar{u}\,\bar{c} + \langle u_{hf} c_{hf} \rangle + \langle u_{lf} c_{lf} \rangle \tag{3}$$

where the ~overbar have been removed and cross-products between high (low) frequency velocity components and low (high) frequency sediment concentration are considered relatively small since they are generally non-correlated.

Oscillatory sediment fluxes at different frequency components are studied using spectral techniques (Huntley and Hanes, 1987) and the cross-spectrum of velocity and concentration (*u*-*c*) has been computed. The integral of the *u*-*c* co-spectrum at the high and low frequency selected regions provides a good approximation to the time averaged sediment fluxes q_{hf} and q_{lf} in equation (3). Magnitude squared coherence and phase spectrum can be also used to study phase lags and signal coherence at different frequency regions. The cross-spectrum has been computed from velocity and sediment concentration signals using the Fast Fourier Transform with no windowing or frequency smoothing, and averaging between the last 6 hydrodynamics runs. For simplicity, cross-spectrum integrals have been performed at the group frequency and at the primary frequency range, neglecting any other contribution to the sediment transport. Nevertheless, these components represent more than 90% of the total sediment fluxes. Good agreement between the total time-averaged suspended sediment fluxes

computed from the time series and spectral integration was found.

As the interest of this analysis is to study the relative contribution of mean and oscillatory components at the high and low frequency regions, the net sediment fluxes are also expressed as relative quantities to the total sediment mobilized in order to facilitate comparisons between different locations and to reduce variability in the transport rates between different locations or due to small variations on sensor locations relative to the bed level. We denote Q_{bulk} to the total sediment mobilized at each sensor location independently of the sign:

$$Q_{bulk} = |q_m| + |q_{hf}| + |q_{lf}| \tag{4}$$

The normalized suspended sediment fluxes (Φ) are then obtained as (Aagaard and Greenwood, 2008):

$$\Phi_i = \frac{q_i}{Q_{bulk}} \tag{5}$$

where the i-subindex indicates each of the sediment flux components (mean, high or low frequency), note that q_i variables denote time averaged sediment fluxes. Negative signs mean sediment fluxes seaward directed, towards the wave paddle; positive signs meaning onshoreward sediment fluxes.

The relative contribution of the different components to the suspended sediment fluxes per test case and location are showed in Table 3 in magnitudes per unit of the total (Q_{bulk}), while the cross-shore location relative to the initial shoreline and bulk suspended sediment fluxes are illustrated in Table 4. The time averaged suspended sediment flux (q_i) at each location and each component can be obtained by just multiplying the specific normalized sediment flux (Φ_i) obtained in Table 3 and the bulk magnitude (Q_{bulk}) in Table 4. For example, the *hf* time averaged sediment flux is: $q_{hf} = \Phi_{hf} \times Q_{bulk}$.

Interesting information arises from Tables 3 and 4. Firstly, at every location and for every test case, the mean current contribution to the sediment fluxes are consistently the largest

contribution to the bulk sediment flux being in general above 0.7 in magnitude (mean of -0.78) and negative promoting seaward directed sediment transport. The second main contribution is the wave group (*lf*) induced suspended sediment fluxes which accounts for an average of 0.18 in absolute value of the bulk sediment flux, although it shows a larger variability in magnitude and direction. Finally, the smallest contribution to the bulk sediment flux is the high frequency component accounting for an average of a 0.04 of the bulk sediment flux also with some variability in magnitude and sign, depending on sensor location and wave conditions. The three locations show many similar patterns in general, although some differences appear due to differences in the cross-shore location relative to x_0.

The high frequency component is positive most of the time at cases BE1 and BE2 but negative for cases BE3 and BE4, depending on cross-shore location relative to the initial shoreline. The reason behind this is due to the phase-lag between the incident velocity and suspended sediment peaks. In cases BE1 and BE2, the short wave component of velocity is in phase with the major suspended sediment events, onshore *hf* velocity peaks are coincident with the largest concentration peaks at the *hf* range. However, for cases BE3 and BE4, the suspended sediment concentration peaks are generally out of phase with the velocity at the *hf* components.

The *lf* influence is more difficult to interpret due to variations with the cross-shore location relative to x_0 and the long wave cross-shore structure. For BE3 and BE4, q_{lf} is predominantly negative and related to the phase lag between the *lf*-velocities and the *hf*-wave envelope. Wave conditions BE3 and BE4 are characterized by a long wave progressive pattern with a dominance of the ingoing long wave, as discussed in Section 3.5. The long wave is out of phase with the *hf* wave groups at the breaking location but the phase lag reduces progressively in the surf zone. The long wave sediment transport is predominantly negative due to the coincidence of *lf* negative velocities and sediment suspension induced by the large

waves within the group (Aagaard and Greenwood, 2008), and as observed in Figure 15.

In contrast, q_{lf} for cases BE1 and BE2 is predominantly positive due to the generally coincidence of positive *lf* velocities and larger SSC events (see Figure 14). Wave conditions BE1 and BE2 are characterized by a standing long wave pattern and the phase lag between the *lf* water surface and velocity signals is due to the ingoing-outgoing influence in the velocity signal via the long wave phase velocity. Nevertheless, for all tested wave conditions and at the selected cross-shore locations the sediment transport is dominated by the mean current induced sediment transport.

4 – Discussion

The experimental data and analysis presented in the present study show a clear influence of the wave group modulation in the breaker bar cross-shore migration and in the final bar position at the end of the experimentation time. In this section, relationships between the observed bar morphological behavior, the wave group period and the observed hydrodynamics and sediment transport will be discussed. The wave group period also seems to have an important influence on shoreline erosion and berm morphological evolution but this will not be covered in this study.

It is important to discuss the wave group period influence on the bar migration relative to other parameters such as the dimensionless sediment fall velocity parameter ($\Omega=H/w_sT$). Ω-parameter has been traditionally used to determine the overall beach tendency (erosion or accretion) with respect to wave climate. In the present experimental condition Ω is kept approximately constant by generating wave conditions of very similar energy content within the wave generation limits. Due to the empirical wave paddle transfer function, small variations of Ω appear between wave conditions. This is translated into small variations of the

primary wave height since the sediment size (settling velocity) and primary wave period is kept constant. It is important to highlight that these differences in Ω are not large enough to overcome the wave group period influence in the measured bar migration as it will be shown next.

Similar to Baldock et al. (2011), the measured cross-shore sediment transport rates obtained using the Exner equation (Eq. 1) has been integrated in the cross-shore dimension to obtain an integrated transport rate. Note that the cross-shore sediment transport rate is a vector and its cross-shore integration is non-zero, although the cross-shore integration of the bed level changes (Δz) is zero due to sediment mass continuity. Integrated sediment transport rates are normalized with the maximum value (found for BE3 case). Figure 16a displays the final cross-shore bar location and mean primary breaking location with respect to the wave group period, Ω-values are displayed in the background as bar plots. Figure 16a shows a clear relationship between the final bar and wave breaking locations with the wave group period, increasing the bar and wave breaking locations as the wave group period increases. The Ω parameter shows to have no apparent influence on the final bar location. On the other hand, Figure 16b shows the normalized integrated sediment transport as a function of Ω, while the group period for each case is displayed in the background as a bar plot. Figure 16 illustrates that the small Ω variations existing between the different wave conditions are not large enough to affect the final cross-shore bar location compared to the wave group period influence. However Ω still controls the integral of the sediment transport rate, interpreted as a measure of the total sediment transport capacity. Note that the Iribarren number is very similar between the different wave conditions (Table 2). Iribarren number has been traditionally used as a descriptor of the type of wave breaking and wave breaking criteria expressed in the form of a wave height to depth ratio (Battjes, 1974). According to the Iribarren numbers displayed in Table 2, the four tested bichromatic conditions should

approximately break in a similar water depth, i.e. cross-shore location since the initial profile is the same, with small variations due to slight differences in Iribarren number and/or primary wave height. Neither the small differences in the Iribarren number or in Ω are reflected in the observed differences in the wave breaking location.

Moreover, it has been shown that, at the breaking location, the wave height tends to be higher for larger wave group periods, as illustrated in the observed larger γ-values for larger values for the wave group period. Therefore, although the Ω parameter is computed using deep water wave heights, a computation of Ω using the wave height at the breaking location ($\Omega_b=H_b/w_sT$ where $H_b=\gamma\ h_b$), seems a better indicator of the observed bar location at increasing distances with respect to the SWL since it includes the group period influence in the wave breaking.

It has been shown that a larger dissipation of the f_1 component (higher frequency component) with respect to f_2 during shoaling is more evident when the frequency difference increases (i.e. broader frequency band with shorter wave group periods). This has been also observed in B00. It has already been postulated to be related to the energy transfer from the primary waves to the bound wave during shoaling implying dissipation of f_1 component. Independently of the selective f_1 dissipation mechanism, the influence on the propagating wave groups is a reduction in the modulation and a decay of the primary wave height during shoaling for broader frequency band components. For a given theoretical bichromatic wave condition composed of two components H_1 and H_2, the maximum modulation is obtained when $H_1/\ H_2 = 1$ and therefore any dissipation in H_1 leads to a modulation reduction. This means that a given energy content is more equally distributed in the waves composing the group structure and a reduction in the maximum wave height for a given energy content. Keeping the mean primary wave period constant, this is translated in a reduction in the steepness of the largest wave heights in the group. Baldock (2012) has also suggested a

decrease in the short wave height amplitude for small wave group periods, which is caused by energy transfer from the higher frequency short wave component (f_1).

For broad banded cases, BE1 and BE2, a reduction in the water surface elevation modulation during wave propagation has been observed whereas narrow banded cases (BE3 and BE4) kept the initial modulation more. Consequently, a reduction in the primary wave height during shoaling has been observed for smaller wave group periods (cases BE1 and BE2) whereas larger wave group periods do not show such wave height decay. These changes in modulation and primary wave height would explain variations in the observed wave breaking.

Previous recent studies in short and long wave propagation over sloping beds (Baldock and Huntley, 2002; Battjes et al. 2004; Janssen et al. 2003 among many others) have focused on the wave group forcing of *lf* waves, *lf* waves growth during shoaling and nearshore dissipation. In these studies the energy loss from short waves is generally assumed small compared to the total short wave energy and not considered. This study suggests that this may not be the case and the energy transfer from short waves to low frequency motions may affect the short wave height cross-shore distribution during shoaling, wave breaking properties and consequently the beach profile evolution.

It has been also observed that increasing the wave group period leads to a general larger variability in the beach profile evolution in terms of bed level changes with experimentation time (as illustrated in Figures 10c and 11c), wave conditions with smaller wave group periods seem to reach to a *quasi-equilibrium* situation faster. This larger variability is observed in the bar morphology in terms of the time evolution of the bar size and location but also in the existing secondary bar and in the inner surf zone bed evolution.

Several studies (Aagaard, 1990; Bauer and Greenwood, 1990; Holman and Bowen, 1982) have reported from field conditions the possibility of suspended sediment convergence at

long water anti-nodal positions contributing to bar migration towards antinode positions or bar maintenance (Symonds and Bowen, 1984). Other studies (Sallenger and Holman, 1987), however do not support that evidences in line with the present experiments where no evidences of an antinode bar migration is found for cases BE3 and BE4. However the present data show a strong link between the wave group modulation, the primary wave breaking location and the final cross-shore location of the breaker bar. Baldock et al (2011) comparing bichromatic wave conditions with monochromatic conditions of similar energetic content, also showed that modulated waves generated a breaker bar located further seaward than the bar observed with the equivalent monochromatic case. They also discussed the influence of wave modulation and the influence of the largest wave within the group in the observed beach profile evolution and breaker bar location.

Ensemble average of hydrodynamics and suspended sediment concentration and time averaged suspended sediment fluxes computed using spectral techniques have shown that, within the surf zone, the mean component is consistently the largest contribution in the net suspended sediment fluxes, and is always directed seaward.

Suspended sediment fluxes computed from co-spectral analysis of velocity and SSC time series suggest a more negative tendency (seaward sediment fluxes) in the *lf*-induced sediment fluxes for narrow banded conditions (BE3 and BE4) in most locations within the inner surf zone due to the progressive cross-shore structure of the *lf* motions. This may have an influence on the measured bar migration if this tendency is maintained close to the breaking location. The present data, however do not clarify this.

Therefore, it is postulated that the wave group propagation and earlier breaking for larger wave group periods largely explain the observed variation in the breaker bar location. Earlier wave breaking is associated with a seaward displacement in the location of the maximum value of the mean return flow. The cross-shore gradients in the undertow-induced sediment

transport result in erosion onshore of the bar crest, and deposition offshore of the sandbar crest, and thus, offshore bar migration with increasing distances relative to the SWL for larger wave group periods. Larger variability in the breakpoint location and a more negative tendency (seaward sediment fluxes) in the *lf*-induced sediment fluxes for narrow banded conditions (larger wave group period) would also facilitate this behavior.

Finally, it is also important to discuss about the wave generation and the presence of energy as free ingoing long wave at f_g by reflection at the wave paddle ("seiching") as active wave absorption was not possible at the selected f_g values. It has been shown that, for larger wave group periods (BE3 and BE4), the long wave height cross-shore structure during shoaling shows the pattern of a progressive long wave dominated by the incident bound wave and not evidences of seiching. However, for shorter wave group periods (BE1 and BE2) the incident free long wave is also important. Propagation of free long wave components to the primary breaking point revealed that free incident ingoing long wave represent up to 27% of the total energy at the group frequency. It is unlikely that this re-reflected long wave will have a strong influence on the bar morphological evolution.

Active wave absorption systems have been applied in many small to medium scale experiments to reduce the influence of the reflected waves at the wave paddle. However, note that under small to medium scale conditions active wave paddle absorption systems have reported an absorption effectiveness decreasing as the wave group frequency reduces, with effectiveness of 90% (in amplitude terms) of reflected waves for frequencies at above 0.4Hz, decreasing to over 60% at 0.1Hz (B00). This efficiency decrease is evident since larger long waves (decreasing f_g) implies larger paddle strokes. In this sense it is highly difficult to absorb the wave group frequencies generated in this work (f_g~ 0.0667 Hz – 0.0361 Hz). For the generated group frequencies long wave lengths oscillates between 73 m and 130 m at the toe of the wave maker where h = 2.5 m. Similar group frequencies at smaller water depths

(smaller scale) results in reduced wave length and long wave momentum to be absorbed by the wave paddle.

Long wave absorption seems, then, a clear limitation of this type of large scale experimentation. However large-scale experimentation offers important and evident advantages in sediment dynamics studies as for example allowing sediment mobility closer to real conditions and larger Reynolds numbers.

In this study, a quantification of the energy reflected at the wave paddle has been attempted by ingoing-outgoing separation at the constant depth section. This separation is feasible with bichromatic wave conditions. It is unlikely that the incident free long wave has an important influence on the primary wave height breaking and the proposed mechanism behind the observed breaker bars distances to SWL as the wave group period increases. The amplitude of the incident free long wave is relatively small to promote differences in the wave breaking location or to mobilize sediment although it may influence the long wave induced sediment transport. Differences in wave breaking locations are explained due to differences in energy transfer from primary components to the bound long wave which travel with the wave groups, where the incident free long wave is theoretically not involved.

5 – Conclusion

Large-scale laboratory measurements of beach profile evolution, hydrodynamics and sediment concentration have been presented showing the influence of wave group periods in the measured beach profile morphological evolution. Four different bichromatic conditions with similar energy content but varying the bichromatic bandwith have been tested. The measured beach profile evolution shows important differences explained from the wave group modulation. It has been shown that increasing the wave group period promotes a larger variability in the profile evolution and the breaker bars to be located further seaward with respect to the initial shoreline.

Measured wave height to depth ratios (γ) show increasingly larger γ-values as the wave group period increases and earlier wave breaking for larger wave group periods. The earlier wave breaking for narrow bandwidth conditions (larger wave groups) is explained by a similar dissipation of the primary wave components during shoaling and maintenance of the modulation structure during shoaling compared with broader bandwidth conditions. Broader bandwidth (smaller wave group periods) have shown a larger dissipation of the higher primary wave component (f_1) with the consequent reduction in wave modulation and primary wave height decay during shoaling.

Moreover, the relative contribution of mean, primary waves and wave group components to the suspended sediment fluxes have been computed using spectral techniques. It has been shown that the mean component dominates the suspended sediment transport in the selected locations within the surf zone and consistently inducing negative sediment fluxes (seaward directed). The different seaward migration for the different wave group periods is then explained by the influence of the seaward displacement of the breakpoint and breaking induced return current as the wave group period increases. The standing-progressive pattern of the *lf* motions and the resultant *lf*-induced sediment transport may also play a role. However, these two contributions seem of minor importance within the inner surf zone relative to the mean induced sediment transport, and measurements close to the bar were not available.

Acknowledgments

The experimental part of this work was funded by European Community's Seventh Framework Programme through the grant to the budget of the Integrating Activity HYDRALAB IV within the Transnational Access Activities, Contract no. 261520. We would like to thank the CIEM staff (Quim Sospedra, Ricardo Torres and Oscar Galego) for their

assistance in running the experiments. Finally, we sincerely thank the reviewers for suggesting substantial improvements.

References

Aagaard, T., 1990. Infragravity waves and nearshore bars in protected, storm-dominated coastal environments. Marine Geology, 94(3): 181-203.

Aagaard, T. and Greenwood, B., 1994. Suspended sediment transport and the role of infragravity waves in a barred surf zone. Marine Geology, 118: 23-48.

Aagaard, T. and Greenwood, B., 2008. Infragravity wave contribution to surf zone sediment transport — the role of advection. Marine Geology, 251: 1-14.

Alsina, J.M. and Baldock, T.E., 2007. Improved representation of breaking wave energy dissipation in parametric wave transformation models. Coastal Engineering, 54(10): 765-769.

Alsina, J.M. and Cáceres, I., 2011. Sediment suspension events in the inner surf and swash zone. Measurements in large-scale and high-energy wave conditions. Coastal Engineering, 58(8): 657-670.

Alsina, J.M., Cáceres, I., Brocchini, M. and Baldock, T.E., 2012. An experimental study on sediment transport and bed evolution under different swash zone morphological conditions. Coastal Engineering, 68(0): 31-43.

Baldock, T.E., 2012. Dissipation of incident forced long waves in the surf zone—implications for the concept of "bound" wave release at short wave breaking. Coastal Engineering, 60: 276-285.

Baldock, T.E. and Huntley, D.A., 2002. Long-wave forcing by the breaking of random gravity waves on a beach. Proceedings of the Royal Society of London A, 458(2025): 2177-2201.

Baldock, T.E., Huntley, D.A., Bird, P.A.D., O'Hare, T.J. and Bullock, G.N., 2000. Breakpoint generated surf beat induced by bichromatic wave groups. Coastal Engineering, 39(2-4): 213-242.

Baldock, T.E., Alsina, J.A., Caceres, I., Vicinanza, D., Contestabile, P., Power, H. and Sanchez-Arcilla, A., 2011. Large-scale experiments on beach profile evolution and surf and swash zone sediment transport induced by long waves, wave groups and random waves. Coastal Engineering, 58(2): 214-227.

Battjes, J.A., 1974. Surf similarity. Proceedings of 14th Coastal Engineering Conference, Copenhagen, Denmark, pp. 466-480.

Battjes, J.A. and Janssen, J.P.F.M., 1978. Energy loss and set-up due to breaking of random waves. 16th International Coastal Engineering Conference, Hamburg, pp. 569-587.

Battjes, J.A., Bakkenes, H.J., Janssen, T.T. and van Dongeren, A.R., 2004. Shoaling of subharmonic gravity waves. Journal of Geophysical Research: Oceans, 109(C2): n/a-n/a.

Bauer, B.O. and Greenwood, B., 1990. Modification of a linear bar-though system by a standing edge wave Marine Geology, 92: 177-204.

Bowen, A.J., 1980. Simple models of nearshore sedimentation: Beach profiles and longshore bars. In: S.B.M. Cann (Editor), The coastline of canada, pp. 1-11.

Brocchini, M. and Peregrine, D.H., 1996. Integral flow properties of the swash zone averaging. Journal of Fluid Mechanics, 317: 241-273.

Cáceres, I. and Alsina, J.M., 2016. Suspended sediment transport and beach dynamics

induced by monochromatic conditions, long waves and wave groups. Coastal Engineering, 108: 36-55.
Dean, R.G., 1973. Heuristic models of sand transport in the surf zone. Engineering Dynamics of the Coastal Zone: First Australian Conference on Coastal Engineering, Sydney, pp. 208–214.
Deigaard, R., Jakobsen, J.B. and Fredsøe, J., 1999. Net sediment transport under wave groups and bound long waves. Journal of Geophysical Research: Oceans, 104(C6): 13559-13575.
Downing, J.P. and Beach, R.A., 1989. Laboratory apparatus for calibrating optical suspended solids sensors. Marine Geology, 86(2–3): 243-249.
Dubarbier, B., Castelle, B., Marieu, V. and Ruessink, G., 2015. Process-based modeling of cross-shore sandbar behavior. Coastal Engineering, 95(0): 35-50.
Elgar, S. and Guza, R.T., 1985. Observations of bispectra of shoaling surface gravity waves. Journal of Fluid Mechanics, 161: 425-448.
Freilich, M.H. and Guza, R.T., 1984. Nonlinear effects on shoaling surface gravity waves, 311, 1-41 pp.
Holman, R.A. and Bowen, A.J., 1982. Bars, bumps and holes: Models for the generation of complex beach topography. Journal of Geophysical Research, 87: 457-468.
Huntley, D.A. and Hanes, D.M., 1987. Direct measurement of suspended sediment transport, Proc. Coastal Sediments'87. A. soc. Civ. Eng. , New York, pp. 723-737.
Janssen, T.T., Battjes, J.A. and van Dongeren, A.R., 2003. Long waves induced by short-wave groups over a sloping bottom. Journal of Geophysical Research, 108(C8): 3252, doi:10.1029/2002JC001515, 8-1 to 8-14.
Kostense, J.K., 1984. Measurements of surf beat and setdown beneath wave groups. Proc. of the International Conference on Coastal Engineering, pp. 724-740.
List, J.H., 1992. A model for the generation of two-dimensional surf beat. Journal of Geophysical Research, 97(C4): 5623-5635.
Longuet-Higgins, M.S. and Stewart, R.W., 1962. Radiation stress and mass transport in gravity waves, with application to `surf beats'. Journal of Fluid Mechanics, 13: 481-504.
Longuet-Higgins, M.S. and Stewart, R.W., 1964. Radiation stresses in water waves; a physical discussion with applications. Deep-Sea Research, 11: 529-562.
Madsen, P.A., Sorensen, O.R. and Schaffer, H.A., 1997. Surf zone dynamics simulated by a boussinesq type model. Part ii: Surf beat and swash oscillations for wave groups and irregular waves. Coastal Engineering, 32(4): 289-319.
O'Hara Murray, R.B., Hodgson, D.M. and Thorne, P.D., 2012. Wave groups and sediment resuspension processes over evolving sandy bedforms. Continental Shelf Research, 46(0): 16-30.
Osborne, P.D. and Greenwood, B., 1992. Frequency dependent cross-shore suspended sediment transport. 2. A barred shoreface. Marine Geology, 106(1-2): 25-51.
Roelvink, D., Reniers, A., van Dongeren, A., van Thiel de Vries, J., McCall, R. and Lescinski, J., 2009. Modelling storm impacts on beaches, dunes and barrier islands. Coastal Engineering, 56(11-12): 1133-1152.
Ruessink, B.G., Houwman, K.T. and Hoekstra, P., 1998. The systematic contribution of transporting mechanisms to the cross-shore sediment transport in water depths of 3 to 9 m. Marine Geology, 152(4): 295-324.
Sallenger, A.H. and Holman, R.A., 1987. Infragravity waves over a natural barred profile. Journal of Geophysical Research: Oceans, 92(C9): 9531-9540.
Sheremet, A., Guza, R.T., Elgar, S. and Herbers, T.H.C., 2002. Observations of nearshore infragravity waves: Seaward and shoreward propagating components. Journal of

Geophysical Research: Oceans, 107(C8): 10-1-10-10.
Shi, N.C. and Larsen, L.H., 1984. Reverse sediment transport induced by amplitude modulated waves. Marine Geology, 54: 181-200.
Svendsen, I.A. and Veeramony, J., 2001. Wave breaking in wave groups. Journal of Waterway, Port, Coastal, and Ocean Engineering, 127(4): 200-212.
Symonds, G. and Bowen, A.J., 1984. Interactions of nearshore bars with incoming wave groups. Journal of Geophysical Research: Oceans, 89(C2): 1953-1959.
Symonds, G., Huntley, D.A. and Bowen, A.J., 1982. Two-dimensional surf beat: Long wave generation by a time varying breakpoint. Journal of Geophysical Research, 87: 492-498.
van Dongeren, A.R., 1997. Numerical modelling of quasi-3d nearshore hydrodynamics Research Report CACR-97-04, Cent. for Appl. Coastal Research, Univ. of Delaware, Newark.
van Dongeren, A.R., Bakkenes, H.J. and Janssen, T.T., 2002. Generation of long waves by short wave groups. Proc. of the Int. Conf. on Coastal Engineering, pp.

List of Figures and Tables

Table 1 - Cross-shore and vertical positions of the different measuring instruments relative to the absolute wave flume cross-shore coordinates (horizontal) and beach bed level (vertical).

Sensor	Nº	x cross-shore position (in m) respect to the wave paddle location (X_a) (elevation relative to the bed level in m, when relevant)
WG	12	7.72, 26.98, 28.48, 30.55, 44.54, 47.54, 50.57, 53.57, 56.59, 59.57, 62.63, 65.61
AWG	8	75.10, 75.86, 76.93, 77.89, 78.41, 79.27, 80.24, 81.34
PPT	8	64.26(0.16), 66.17(0.03), 67.74(-0.11), 69.07(-0.19), 70.27(-0.04), 71.77(-0.12), 73.39(-0.11), 74.24(-0.08)
ADV	7	71.85(0.05), 73.44(0.05), 74.82(0.05), 75.36(0.05), 75.81(0.03), 76.91(0.03), 77.85(0.03)
OBS	8	71.85(0.05), 73.44(0.05), 74.82(0.05), 75.36(0.05), 75.81(0.03), 75.81(0.05), 76.91(0.03), 77.85(0.03)
CCM tanks	2	75.81, 77.84

Table 2 - Generated wave conditions with wave height obtained from spectral moment at the sensor located closest to the wave paddle.

Wave Conditions	**Component 1**		**Component 2**					
	H_1 **(m)**	f_1 **(Hz)**	H_2 **(m)**	f_2 **(Hz)**	Δf **(Hz)**	H/w_sT	**Iribarren**	d **(m)**
BE1	0.29	0.303	0.26	0.237	0.0667	3.08	0.40	2.53
BE1_2	0.30	0.303	0.26	0.237	0.0667	3.12	0.40	2.48
BE2	0.26	0.300	0.24	0.240	0.0600	2.81	0.42	2.5
BE3	0.31	0.295	0.31	0.246	0.0500	3.52	0.37	2.5
BE4	0.29	0.288	0.27	0.252	0.0361	3.13	0.40	2.5
BE4_2	0.28	0.288	0.30	0.252	0.0361	3.27	0.39	2.46

Table 3 - Contributions to the normalized suspended sediment fluxes (Φ) induced by mean, primary waves and wave group components at each wave condition and different cross-shore locations within the inner surf zone.

Wave conditions	Location1 X = 71.85 m, Z = 0.05 m			Location2 X = 73.44 m, Z = 0.05 m			Location3 X = 74.82 m, Z = 0.05 m		
	Φ_m	Φ_{hf}	Φ_{lf}	Φ_m	Φ_{hf}	Φ_{lf}	Φ_m	Φ_{hf}	Φ_{lf}
BE1	-0.82	0.04	0.14	-0.71	0.09	0.20	-0.87	0.05	0.08
BE1_2	-0.78	0.05	0.17	-0.69	0.05	0.25	-0.89	0.00	-0.10
BE2	-0.88	0.02	0.10	-0.53	0.06	0.41	-0.61	0.11	0.28
BE3	-0.87	-0.05	-0.08	-0.87	-0.01	-0.11	-0.75	0.01	-0.24
BE4	-0.90	-0.04	0.07	-0.85	-0.02	-0.12	-0.81	-0.01	-0.18
BE4_2	-0.78	0.01	-0.21	-0.74	-0.06	-0.20	-0.71	-0.04	-0.25

Table 4 - Total absolute suspended sediment mobilized at each sensor location, and sensor cross-shore location relative to the SWL at the initial 1:15 beach profile.

Wave conditions	Location1 X = 71.85 m	Q_{bulk} (m/s)	Location 2 X = 73.44 m	Q_{bulk} (m/s)	Location3 X = 74.82 m	Q_{bulk} (m/s)
BE1	-4.13	1.685	-2.54	1.024	-1.16	0.835
BE1_2	-3.41	1.813	-1.82	1.155	-0.44	0.832
BE2	-3.76	2.406	-2.17	1.349	-0.79	0.542
BE3	-3.62	0.189	-2.03	0.213	-0.65	0.380
BE4	-3.51	0.913	-1.92	0.126	-0.54	0.113
BE4_2	-3.16	0.116	-1.57	0.120	-0.19	0.171

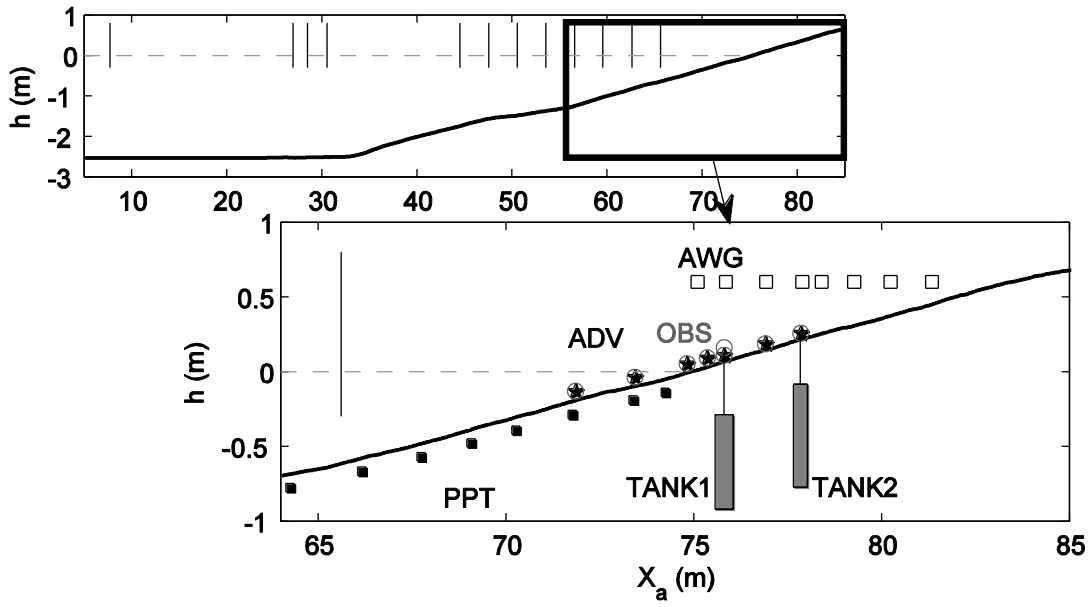

Figure 1 - Wave flume configuration with measured bathymetry averaged over all initial profiles used during the experiments. General view with resistive wave gauge positions, and amplification of the inner surf, swash zones with instrument locations. Solid squares are Pore Pressure Transducers (PPT), open squares are Acoustic Wave Gauges (AWG), open circles correspond to Optical Backscatter Sensors (OBS) and stars symbols mean Acoustic Doppler Velocimeters (ADV).

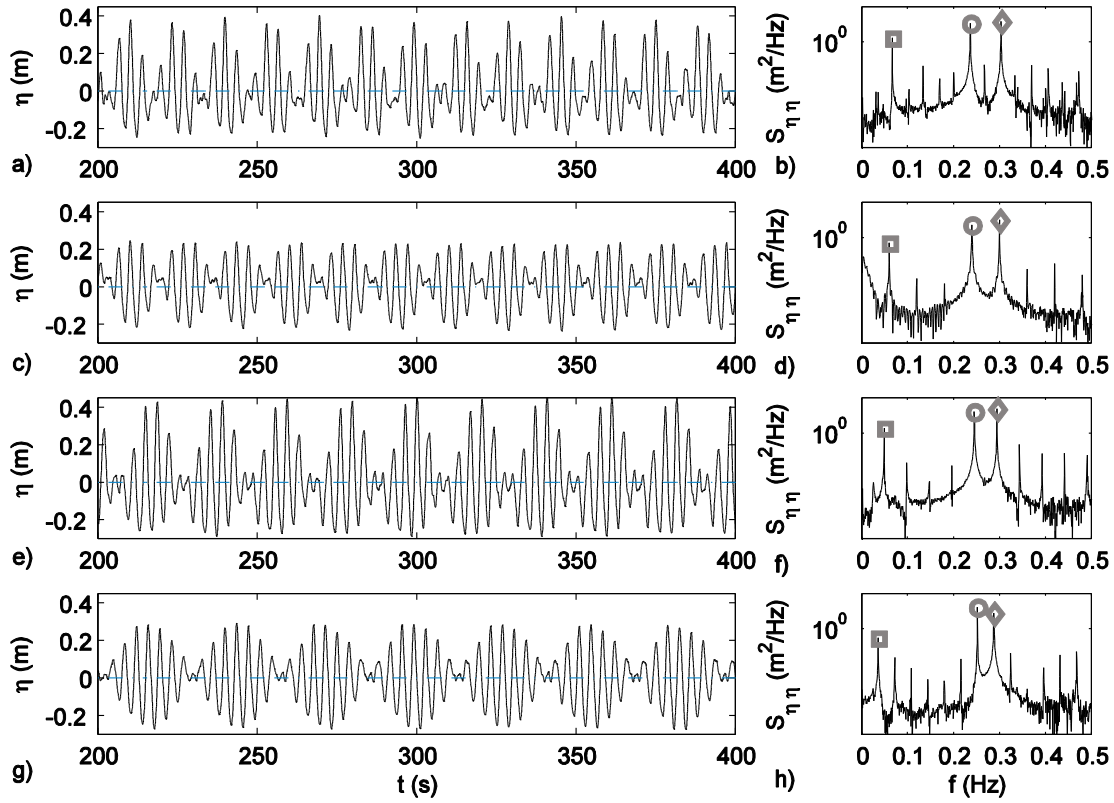

Figure 2 - Time series of water surface elevation measured at X_a = 7.70m (left panels) and computed power spectrum density (right panels) for the different bichromatic conditions: BE1 (a-b), BE2 (c-d), BE3 (e-f) and BE4 (g-h). Symbols in the spectrum plots indicate peaks of energy at frequencies: □ f_g, ◇ f_1 and ○ f_2.

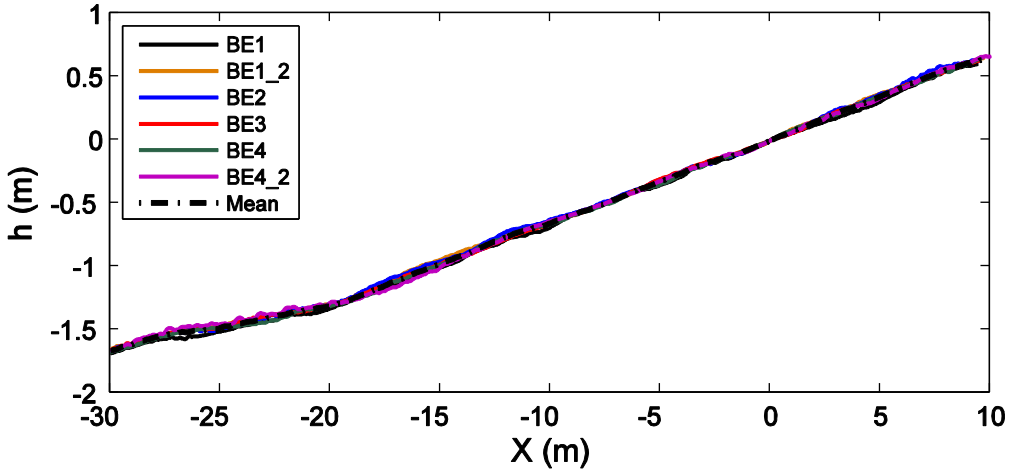

Figure 3 - Measured initial beach profiles during CoSSedM experiments.

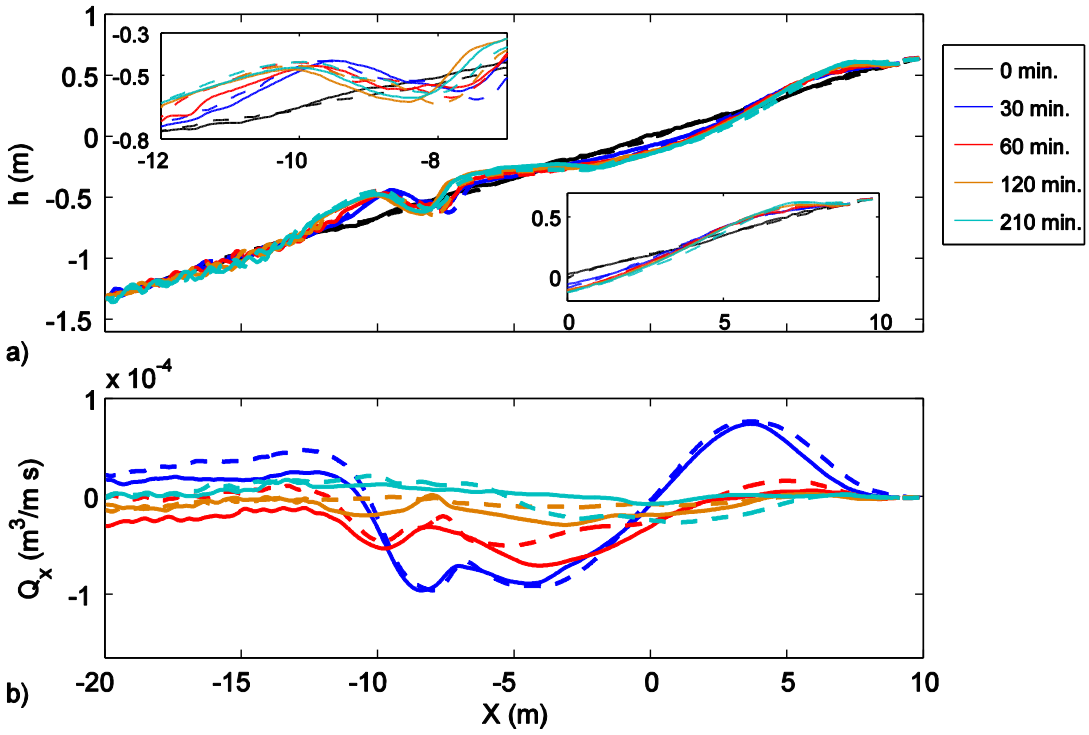

Figure 4 - (a) Beach profile evolution and (b) computed sediment transport rates at different experimentation times for BE1 (solid line) and BE1_2 (dotted line) wave conditions with wave flume working water depths of 2.53 and 2.48 m respectively.

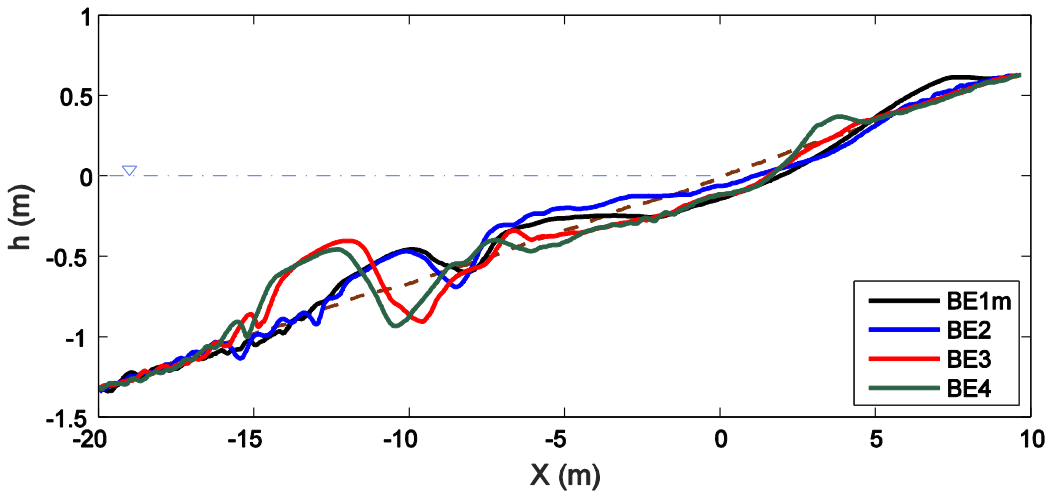

Figure 5 - Mean initial beach profile (dash line) and profile evolution for the different wave conditions after 210 min of wave action.

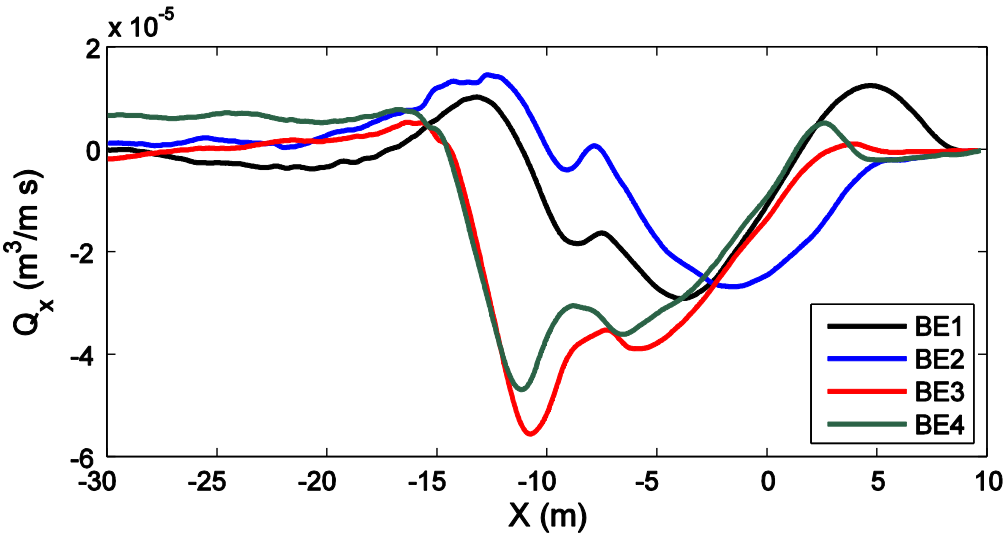

Figure 6 - Cross-shore distribution of computed sediment transport rates using the Exner equation for different wave conditions after 210 min of experimentation time.

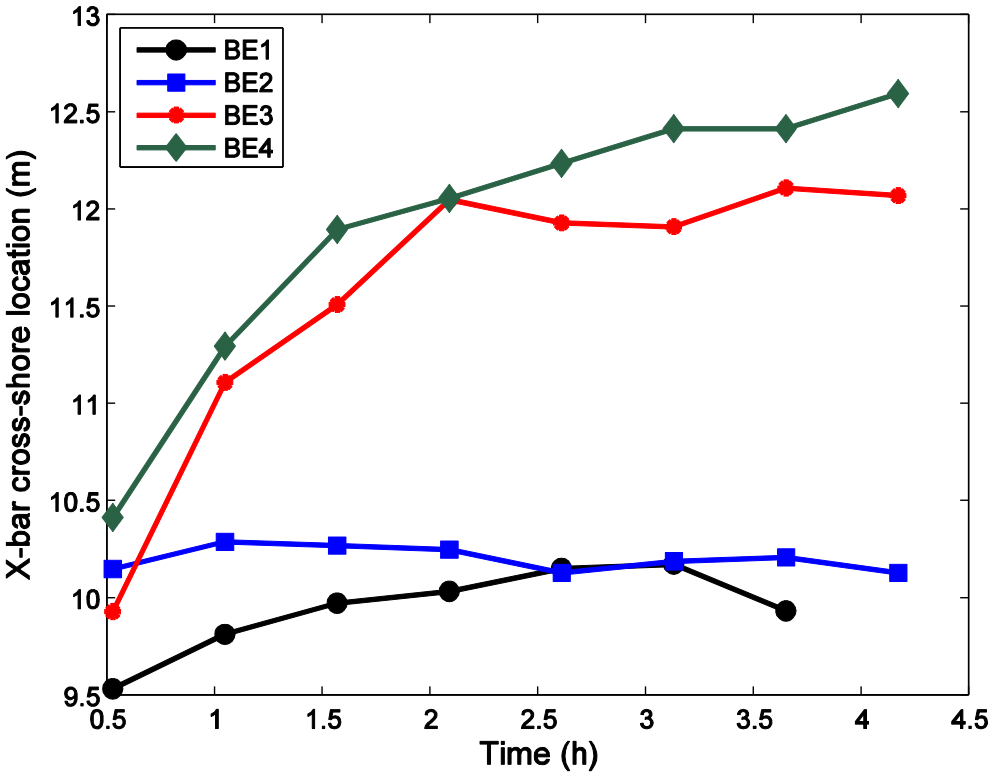

Figure 7 - Time distribution of the main bar crest cross-shore location respect to SWL for the different wave conditions.

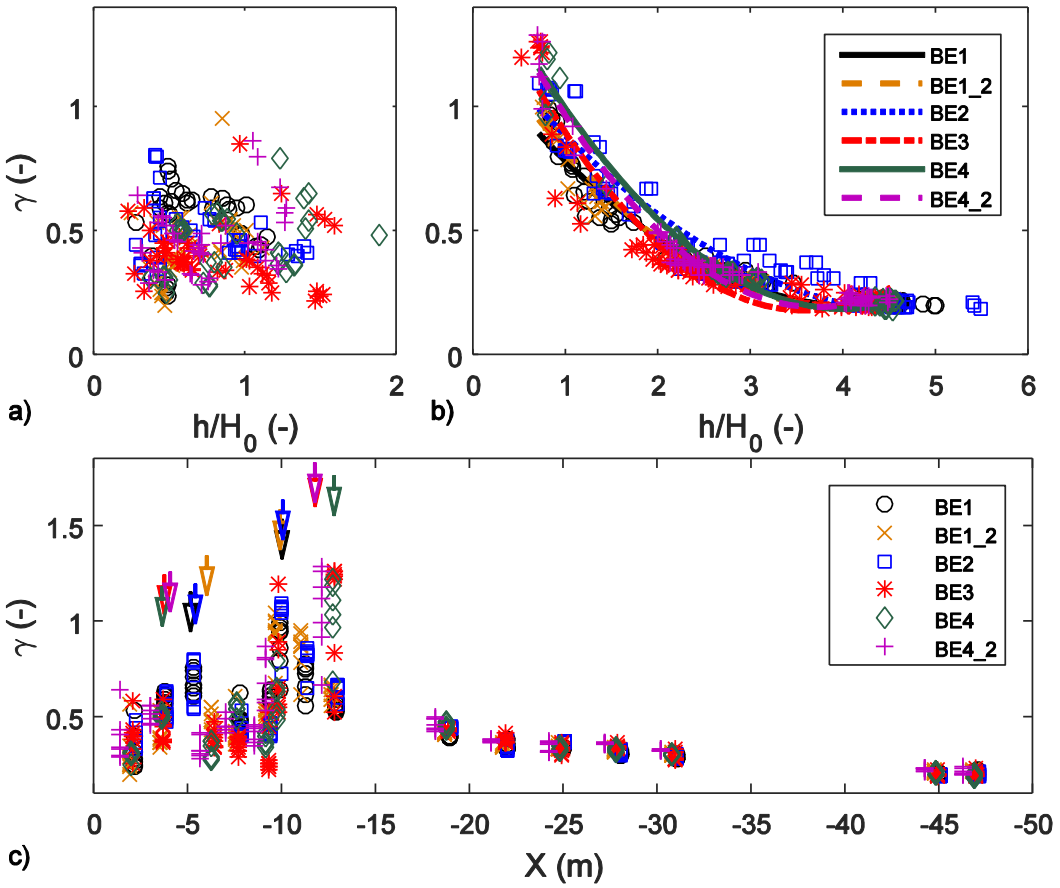

Figure 8 - Distribution of the incident primary wave height to total depth ratio (γ) with respect to (a) the total water depth non-dimensionalised by the initial wave height, and up to the primary wave breaking location; (b) within the inner surf zone; and (c) γ-distribution with respect to the cross-shore location for cases: ○ BE1, × BE1_2, □ BE2, ∗ BE3, ◇ BE4 and +BE4_2. Primary and inner wave breaking locations are indicated with arrows.

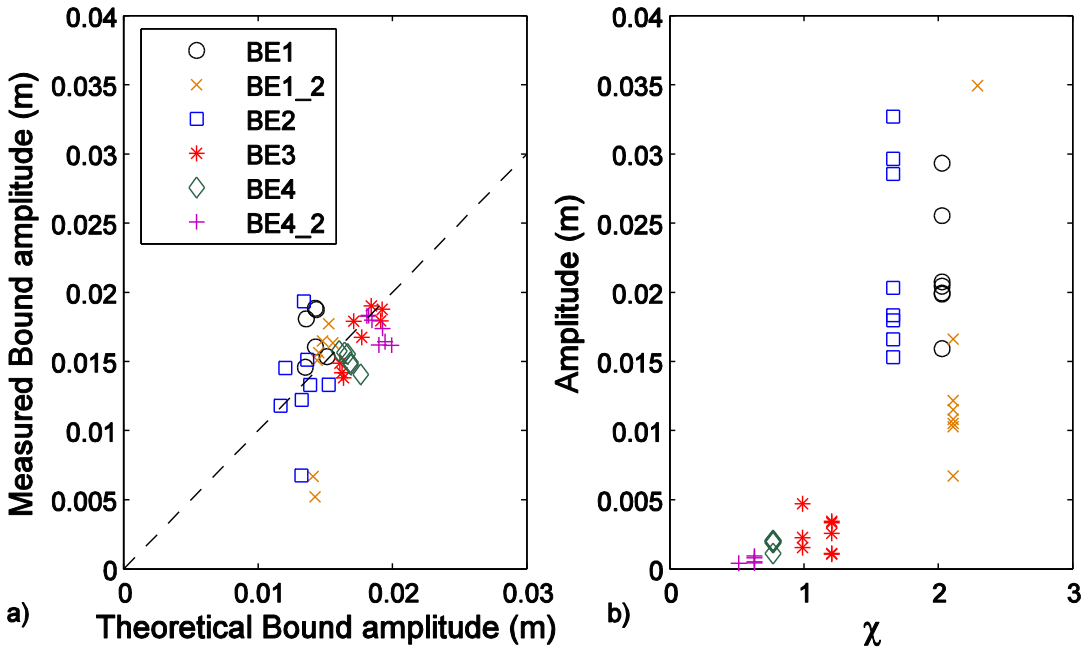

Figure 9 - (a) Comparison of measured and theoretical bound long wave at the group frequency and (b) Outgoing free long wave at the group frequency distribution versus χ parameter, ○ BE1, × BE1_2, □ BE2, ∗ BE3, ◇ BE4 and +BE4_2.

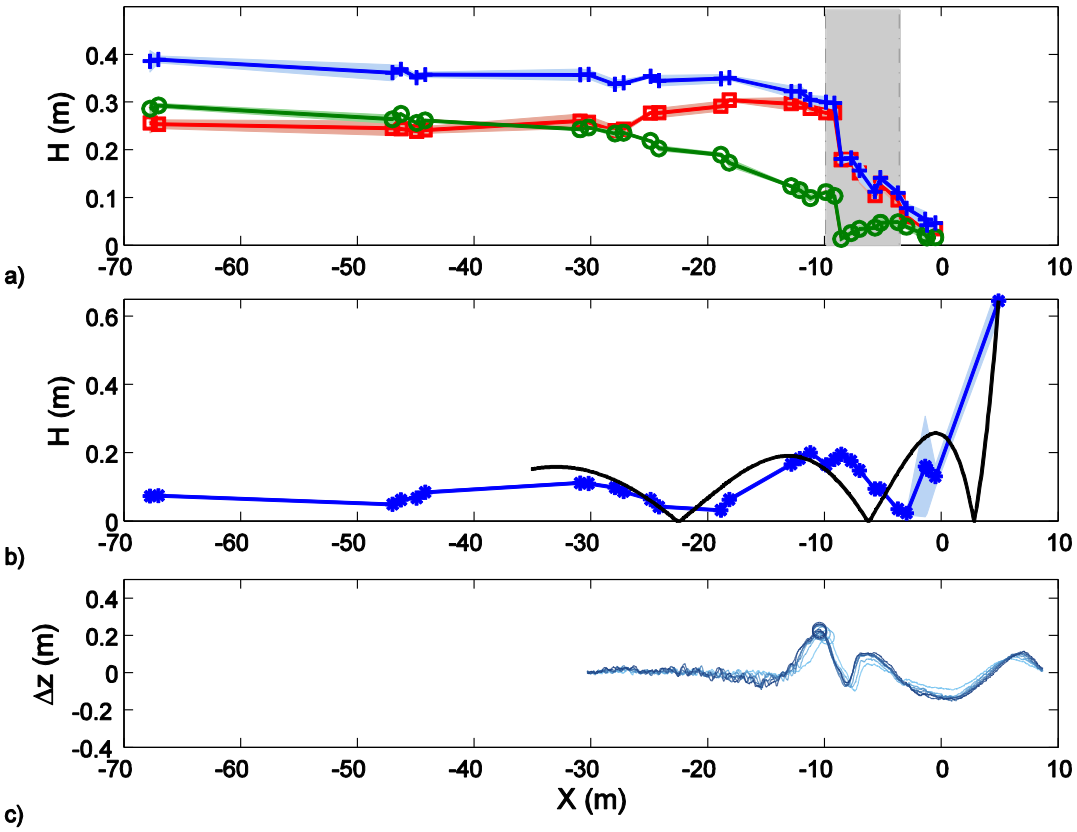

Figure 10 - Cross-shore distribution for tests BE1 and BE1_2 of: (a) measured primary wave height (+), H_1 (○) and H_2 (□) while wave breaking location is indicated in the background with a gray area; (b) measured wave height at f_g (∗) compared to nodal structure of free standing wave (solid line); and (c) Bed level changes respect to initial profile with bar location indicated (○). Wave height variability between hydrodynamic runs is illustrated with a shaded plot while the mean value is indicated with a solid line.

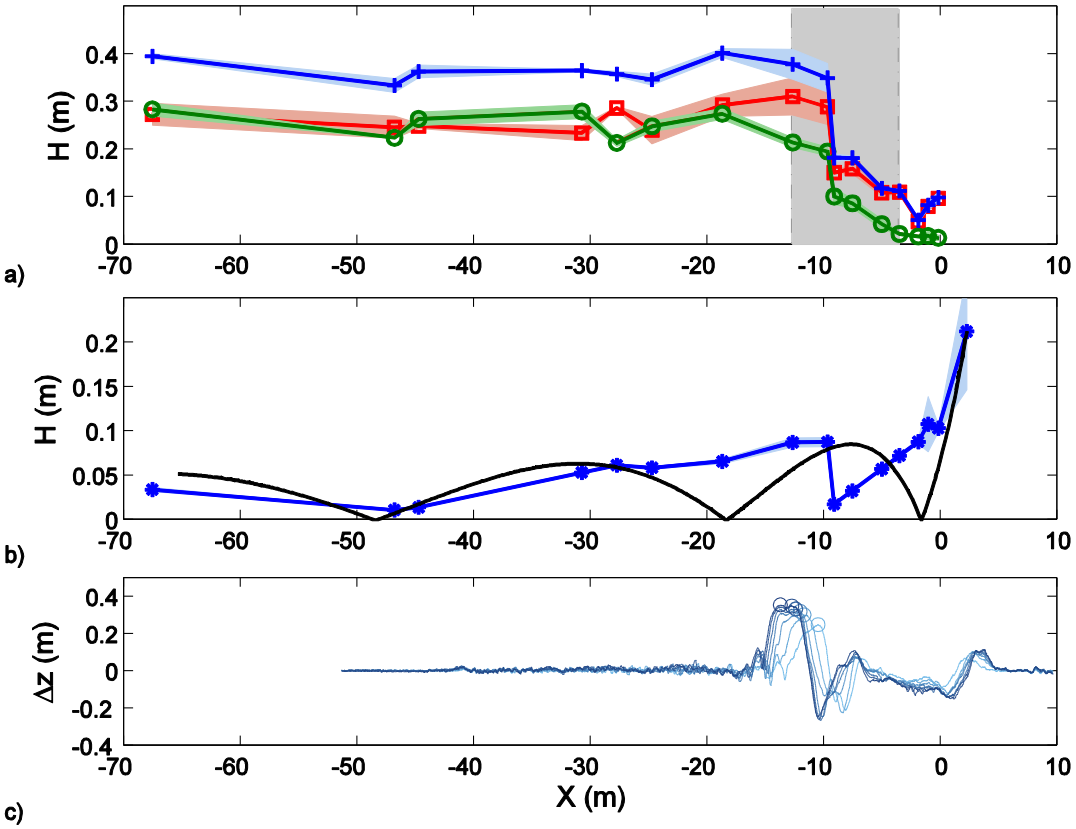

Figure 11 - Cross-shore distribution for test BE4 of: (a) measured primary wave height (+), H_1 (○) and H_2 (□) while wave breaking location is indicated in the background with a gray area; (b) measured wave height at f_g (∗) compared to nodal structure of free standing wave (solid line); and (c) Bed level changes respect to initial profile with bar location indicated (○). Wave height variability between hydrodynamic runs is illustrated with a shaded plot while the mean value is indicated with a solid line.

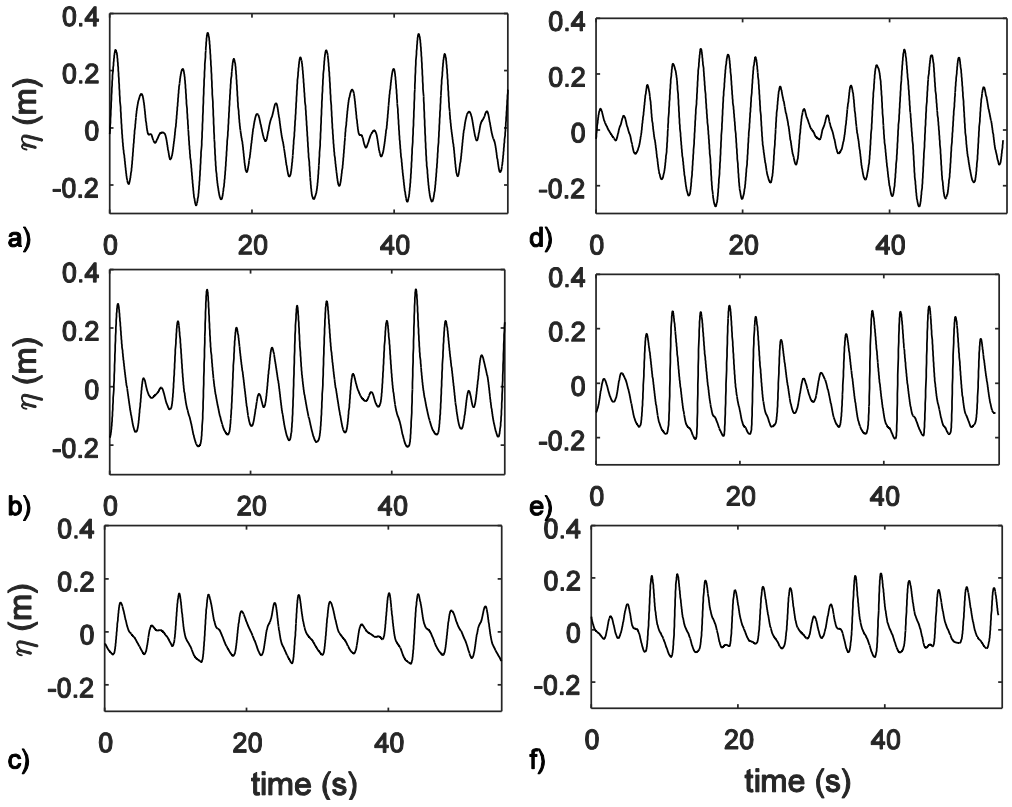

Figure 12 - Ensemble average time distribution of water surface elevations at different cross-shore locations for cases BE1 (a-c) and BE4 (d-f). Cross-shore locations are X = -67.85m (a), -9.96m (b), -7.93m (c), -67.64m (d), -9.75m (e) and -7.625m (f).

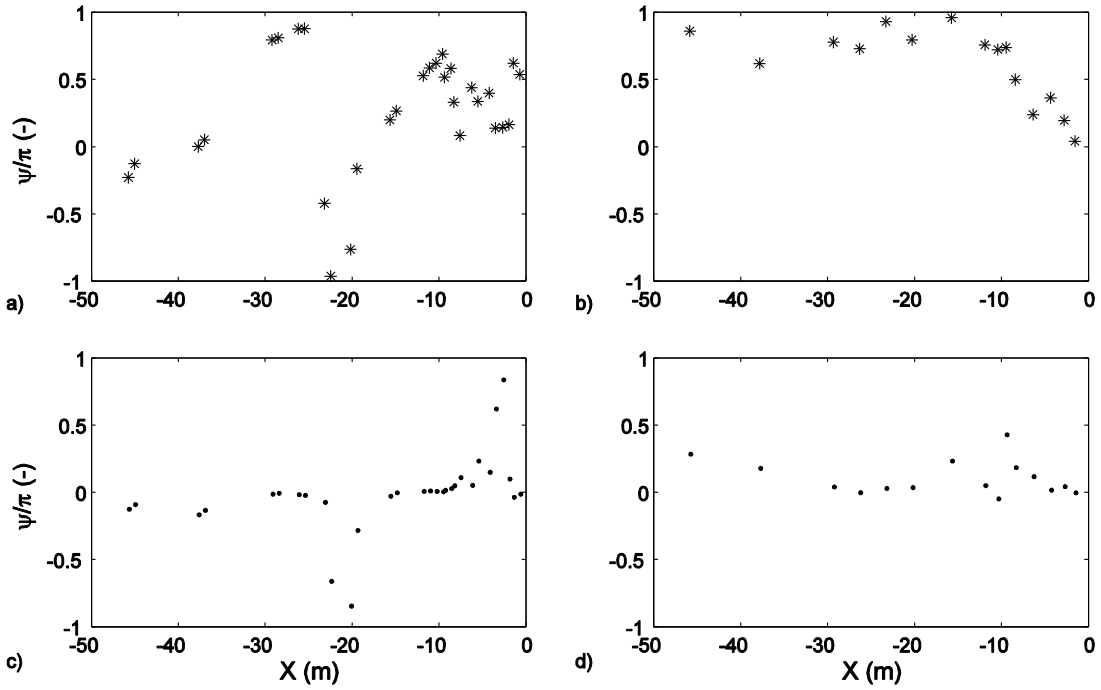

Figure 13 - Phase lag ψ of *lf* waves with respect to *hf* amplitude envelope for cases (a) BE1, BE1_2 and (b) BE4. Phase lag ψ of *lf* waves at consecutive cross-shore locations for cases (c) BE1, BE1_2 and (d) BE4.

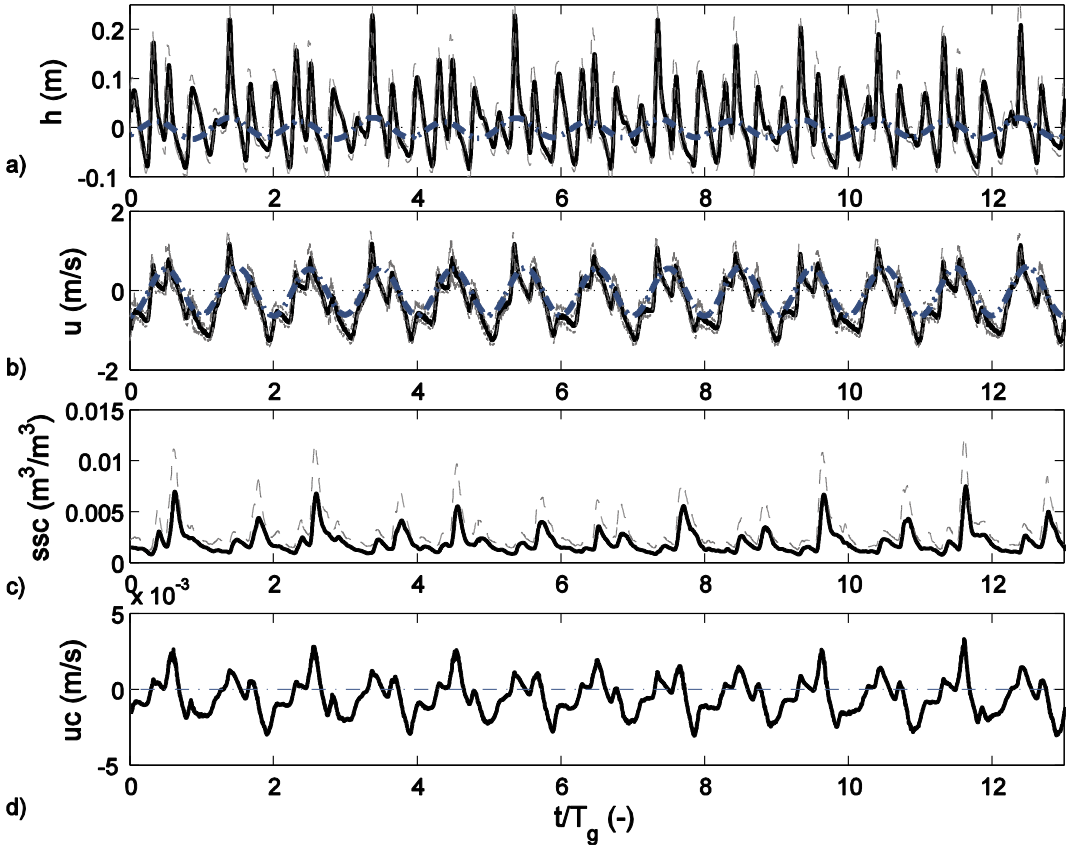

Figure 14 - Ensemble average over the repetition period (T_R) of: (a) water surface elevation, horizontal velocity (b) and (c) suspended sediment concentration at the location x =-4.13 m within the surf zone and wave condition BE1. Solid lines indicate ensemble mean values, dashed lines standard deviation and dash-dotted lines indicate ensemble averaged *lf*-components.

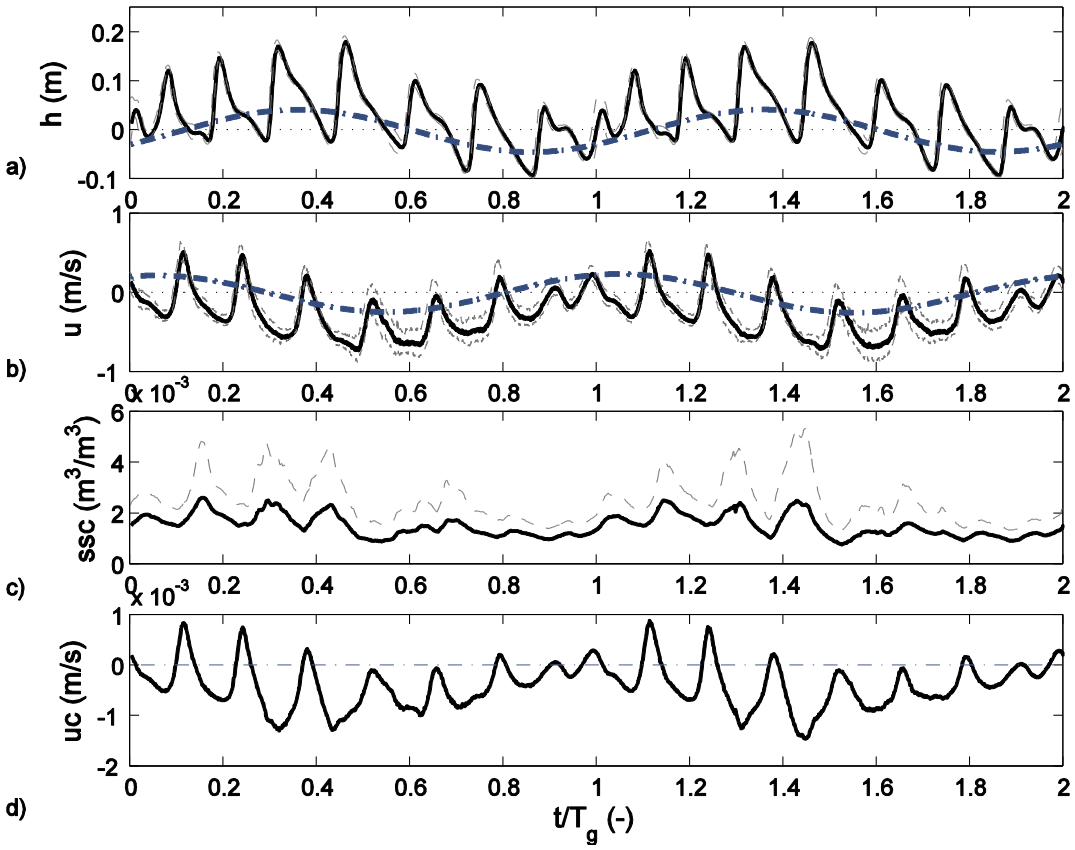

Figure 15 - Ensemble average over the repetition period (T_R) of (a) water surface elevation, horizontal velocity (b) and (c) suspended sediment concentration at the location x =-3.51 m within the surf zone and wave condition BE4. Solid lines indicate ensemble mean values, dashed lines standard deviation and dash-dotted lines indicate ensemble averaged *lf*-components.

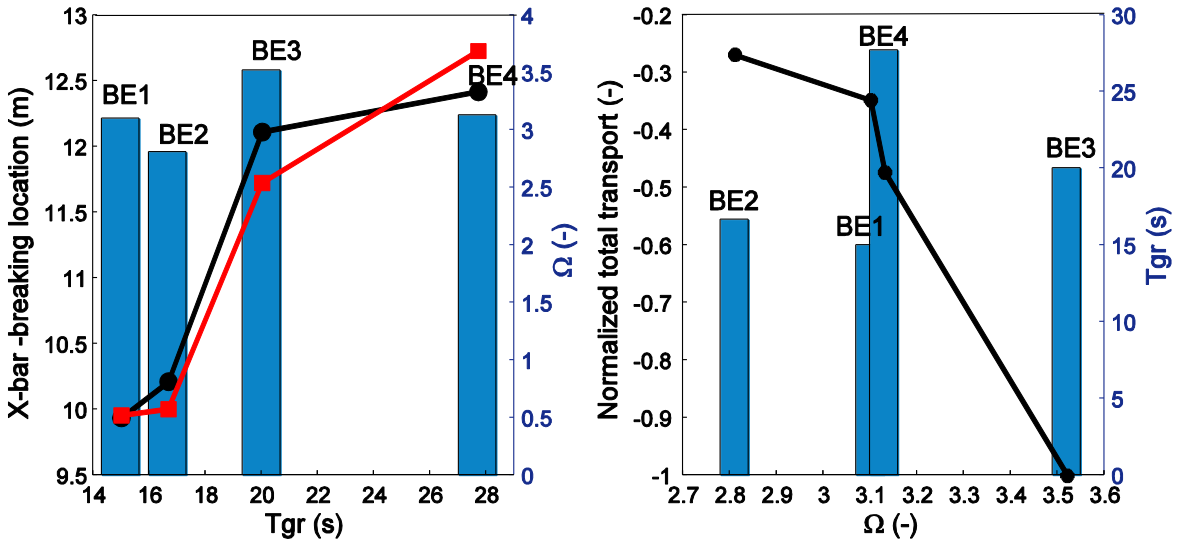

a) b)

Figure 16 - (a) Cross-shore final bar (●) and mean primary wave height location (■) vs wave group period, non-dimensional sediment fall velocity (Ω) is shown with bars; (b) non-dimensional cross-shore sediment transport rates obtained from bed level changes vs Ω (●), wave group period is shown with bars.